Computer Modeling in Engineering & Sciences

Tech Science Press

Doi:10.32604/cmes.2025.060989

ARTICLE

A Numerical Study of the Caputo Fractional Nonlinear Rössler Attractor Model via Ultraspherical Wavelets Approach

Ashish Rayal[1], Priya Dogra[1], Sabri T. M. Thabet[2,3,4,*], Imed Kedim[5] and Miguel Vivas-Cortez[6,*]

[1]Department of Mathematics, School of Applied and Life Sciences, Uttaranchal University, Dehradun, 248007, India
[2]Department of Mathematics, Saveetha School of Engineering, Saveetha Institute of Medical and Technical Sciences, Saveetha University, Chennai, 602105, India
[3]Department of Mathematics, Radfan University College, University of Lahej, Lahej, 73560, Yemen
[4]Department of Mathematics, College of Science, Korea University, Seoul, 02814, Republic of Korea
[5]Department of Mathematics, College of Science and Humanities in Al-Kharj, Prince Sattam bin Abdulaziz University, Al-Kharj, 11942, Saudi Arabia
[6]Faculty of Exact and Natural Sciences, School of Physical Sciences and Mathematics, Pontifical Catholic University of Ecuador, Sede Quito, 17-01-2184, Ecuador

*Corresponding Authors: Sabri T. M. Thabet. Email: th.sabri@yahoo.com; Miguel Vivas-Cortez. Email: mjvivas@puce.edu.ec

Received: 14 November 2024; Accepted: 27 January 2025; Published: 30 May 2025

ABSTRACT: The Rössler attractor model is an important model that provides valuable insights into the behavior of chaotic systems in real life and is applicable in understanding weather patterns, biological systems, and secure communications. So, this work aims to present the numerical performances of the nonlinear fractional Rössler attractor system under Caputo derivatives by designing the numerical framework based on Ultraspherical wavelets. The Caputo fractional Rössler attractor model is simulated into two categories, (i) Asymmetric and (ii) Symmetric. The Ultraspherical wavelets basis with suitable collocation grids is implemented for comprehensive error analysis in the solutions of the Caputo fractional Rössler attractor model, depicting each computation in graphs and tables to analyze how fractional order affects the model's dynamics. Approximate solutions obtained through the proposed scheme for integer order are well comparable with the fourth-order Runge-Kutta method. Also, the stability analyses of the considered model are discussed for different equilibrium points. Various fractional orders are considered while performing numerical simulations for the Caputo fractional Rössler attractor model by using Mathematica. The suggested approach can solve another non-linear fractional model due to its straightforward implementation.

KEYWORDS: Fractional Rössler attractor; ultraspherical wavelets; caputo derivative; error analysis; stability analysis

1 Introduction

In today's world, accuracy is paramount across all fields, making the application of advanced mathematical techniques essential [1–4]. Fractional calculus (FC), an extension of traditional calculus, plays a crucial role in this regard [5–8]. Incorporating fractional derivatives and integrals, FC provides a strong framework for modeling complex systems with memory and inherited features, capturing phenomena that traditional models often overlook [9]. Its applications are increasingly widespread across various fields of science and engineering, offering new insights into real-world challenges. The reach of FC now extends into the areas such as robotics [10], stock market analysis [11], signal processing [12], chaotic dynamical systems [13], image processing [14], viscoelasticity [15], life sciences [16], neural networks [17], pharmacokinetic [18], and

earthquake modeling [19]. This concept enhances the understanding and prediction of systems exhibiting non-local and time-dependent behavior.

Fractional operators [20–22] can be applied in any real or complex order, providing deeper analysis with the flexibility to approach dynamic systems. Fractional integrals generalize traditional integration to non-integer orders, using the Riemann-Liouville [23] or Caputo definitions [24,25]. Integral and differential operators are used in the Liouville and Riemann framework to investigate FC. The Caputo operator is a novel fractional operator that Caputo created, utilizing the framework of FC to study and analyze the models [26,27]. The Caputo fractional derivative is highly regarded as an efficient derivative for real-world applications, as it effectively incorporates initial and boundary conditions. Compared to other fractional derivatives like the Riemann-Liouville derivative, the Caputo derivative avoids certain mathematical complexities, such as needing non-local initial conditions that are more computationally challenging. The use of the Caputo derivative in real-world scenarios often leads to more accurate solutions than other derivatives, when combined with orthogonal polynomials and wavelet-based methods. By incorporating kernel functions that account for historical effects, they effectively model systems with long-range dependencies, such as anomalous diffusion and viscoelastic behavior [28]. Their ability to capture non-local interactions makes them invaluable in fields like physics [29], engineering [30,31], finance [32], and control theory [33] and provide essential tools for understanding complex phenomena. One such tool is a wavelet transform.

Wavelet Transform is a mathematical technique that deals with an expansion of functions as a basis function. Operations on wavelets form wavelets theory [34–36] which can be employed in various fields such as image analysis, control systems, communication systems, stock market analysis, a meteorological model, solutions to differential equations [37,38], and many others [39–41]. In recent years, the wavelets approach has become more and more popular in the areas of numerical methods. Several types of wavelets and function approximation were utilized in these references [42–44]. Wavelet-based approaches are employed for solving differential equations, particularly non-linear differential equations, providing highly accurate solutions by using integration to transform differential equations into integral equations [45–48]. The functions or signals associated with the equations are then compared using truncated orthogonal series expansions. The integral operations within these equations are eliminated by applying an operational matrix of integration, thereby effectively reducing the considered problem to a series of algebraic equations, and simplifying the calculation process. One of its applications includes analyzing chaotic dynamic systems.

Chaotic dynamical systems [49,50] are sensitive to the state of initial conditions applied to the systems. Its characteristics such as unpredictability, sensitivity to initial conditions, and complex dynamics play vital roles in solving real-world scenarios. They are crucial in understanding weather patterns [51], predicting population dynamics [52], encryption in cryptocurrency [53] encryption in image [54], and other fields. In the realm of chaos and dynamical systems, particularly for low-dimensional models, the Lorenz system [55] and Rössler model [56] are two seminal examples that have been widely examined. These models are fundamental in exploring and understanding chaotic dynamics and have contributed a significant role in the advancement of the related fields. The Lorenz system is more complex and closely associated with physical phenomena, generating a double-lobed butterfly attractor representing more intricate chaos. On the other hand, the Rössler system is simpler and serves as an abstract model of chaos, making it ideal for theoretical studies and easier visualizations. It produces a single spiral attractor, which reflects smoother chaos. The coexistence of both asymmetric and symmetric features in the Rössler system allows researchers to explore a broader spectrum of dynamical behaviors as compared to the asymmetric Lorenz system, making it a versatile and insightful model for studying chaotic dynamics. Due to these characteristics, a system of non-linear equation of Rössler attractor model is analyzed numerically in this study by using a wavelet-based technique.

The Rössler system [57] consists of three equations, being one non-linear, three system parameters a, b, c and variables x, y, z representing state variables. The parameter a controls the strength in the y-equation, affecting the rotation in xy-plane, b parameter affects the z-equation, i.e., influences the coupling between x and z components of the system and can be thought of as an external forcing term and c influences the interaction between the x and z variables, controlling the rate at which the z component grows and interacts with the x component. Here $a, b, c \in \mathbb{R}$, and they are assumed to be dimensionless and positive. The Rössler attractor is typically visualized in 3D space with x, y, and z axes, depicting chaotic trajectories that are sensitive and dependent on initial conditions. In this work, the following forms of Caputo fractional Rössler attractor model are considered.

Model 1: Asymmetric fractional Rössler attractor [58]:

$$\begin{aligned} {}_0^C D_\tau^\alpha x(\tau) &= -y(\tau) - z(\tau), \\ {}_0^C D_\tau^\alpha y(\tau) &= x(\tau) + a y(\tau), \qquad \tau \in [0,1], \\ {}_0^C D_\tau^\alpha z(\tau) &= b + z(\tau)(x(\tau) - c), \end{aligned} \tag{1}$$

with the conditions

$$x(0) = x_1, \quad y(0) = y_1, \quad z(0) = z_1. \tag{2}$$

In contrast to the asymmetric Lorenz system, the Rössler system exhibits both symmetry and asymmetry characteristics. Asymmetric Rössler attractor is shown by the model given in Eq. (1). One can change the structure by making changes to the linear or nonlinear variables to build a symmetric system. A 180° rotation around the z-axis corresponds to the system that is invariant undergoing the transformation $(x, y, z) \to (-x, -y, z)$, which can be used to construct a system that is rotationally invariant. System in Eq. (1) requires that some terms be multiplied by suitable variable selections [58].

Model 2: Symmetric fractional Rössler attractor [58]:

$$\begin{aligned} {}_0^C D_\tau^\alpha x(\tau) &= -y(\tau) - y(\tau) z(\tau), \\ {}_0^C D_\tau^\alpha y(\tau) &= x(\tau) + a y(\tau), \qquad \tau \in [0,1], \\ {}_0^C D_\tau^\alpha z(\tau) &= b + z(\tau)((x(\tau))^2 - c), \end{aligned} \tag{3}$$

with the conditions

$$x(0) = x_2, \quad y(0) = y_2, \quad z(0) = z_2. \tag{4}$$

The operator ${}_0^C D_\tau^\alpha$ in Eqs. (1) and (3) represents the fractional derivative in the Caputo sense of order $\alpha \in (0,1]$. The above Caputo fractional Rössler attractor model is an extension of classical Rössler system.

We will utilize the above two systems for our study under the conditions mentioned. Several researchers have studied the above models, their applications, and their nature by utilizing various methods and tools. In [59], Kontorovich et al. used the degenerated cumulant equations method for analysis and provided an application through Rössler attractor output signals to model radio frequency interferences provided by Peripheral Component Interface express. Rysak et al. [60] implemented the Grunwald-Letnikov method for numerical solutions of Caputo fractional Rössler attractor model and did a recurrence quantification analysis. In [61], Elbadri et al. presented a fractional Laplace decomposition technique with an adaptive predictor-corrector algorithm for solving rotationally symmetric Rössler attractor. Kekana et al. [62] conducted the analysis of Rössler attractor by residual and Joubert-Greeff methods. In [63], Barrio et al. studied the regions of parameters for chaotic behavior by using different chaos indicators and conducted a thorough analysis

of the global and local bifurcations of co-dimension one and two of limit cycles. Santra et al. [64] provided the simulation of Rössler attractor through the power series approach. In [65], Boulehmi solved the Caputo fractional Rössler attractor model under the Atangana-Baleanu-Caputo fractional derivative and compared the results with the method.

In this study, we are interested in adapting a novel approach based on ultraspherical Wavelets (USWs) as basis functions for simulating Caputo fractional Rössler attractor model. These wavelets play a significant role in numerical analysis as well as in approximation theory. The importance of studying the fractional Rössler system lies in its potential for better analyzing the applications of such models. To the best of the author's knowledge, this is the first time that the considered model under the Caputo derivative is numerically simulated using USWs. Therefore, motivated by the existing literature, the present work illustrates an application of USWs with collocation nodes to analyze the Caputo fractional Rössler attractor model under the Caputo derivative. An additional motivation is that the Legendre wavelets and Chebyshev wavelets can be inferred as particular instances of the USWs. The presented scheme does not appear to have any significant flaws. However, the suggested scheme works effectively in a limited domain, and processing a large number of USWs could lead to high computational costs. The novelty of this work is presented as:

- The Caputo fractional derivatives have been employed to get more accurate solutions to the Caputo fractional Rössler attractor model.
- The design of the computational framework based on USWs is presented for the first time to solve the Caputo fractional Rössler attractor model numerically.
- The relative representations have been presented through relative errors and L_2 error, which improve the strength of the computing structure USWs to solve the Caputo fractional Rössler attractor model.
- A detailed error and equilibria analysis of the proposed model is provided in this study.

This work is organized as follows: Section 2 presents the fundamental ideas about fractional Caputo operators employed in this work. The USWs basis and approximation of function by USWs are described in Section 3. The USWs technique for simulating Caputo fractional Rössler attractor model is presented in Section 4. Section 5 provides the error and equilibria analysis. The nonlinear Caputo fractional Rössler attractor model is numerically analyzed in Section 6, showcasing results in tables and graphs that demonstrate the effectiveness of the suggested scheme. Section 7 contains the concluding remarks and the future scope.

2 Mathematical Preliminaries

Some preliminaries and notations about FC are included in this section. This work employs the following fractional operators.

Definition 2.1. The fractional Caputo derivative of a function $h(\tau)$ defined on $[0,1]$ with order $\alpha \in (0,1]$ is given by [66]

$$ {}_{0}^{C}D_{\tau}^{\alpha}h(\tau) = \frac{1}{\Gamma(1-\alpha)}\int_{0}^{\tau} h'(t)(\tau-t)^{-\alpha}dt, \quad 0 < \alpha < 1. \tag{5}$$

Definition 2.2. For a function $h(\tau)$, the fractional integral with α order is expressed by [66]

$$ {}_{0}^{C}I_{\tau}^{\alpha}h(\tau) = \frac{1}{\Gamma(\alpha)}\int_{0}^{\tau} (\tau-t)^{\alpha-1}h(t)dt, \quad 0 < \tau, \ \alpha \in (0,1]. \tag{6}$$

- For $0 < \alpha \leq 1$, the relationship between the operators in Eqs. (5) and (6) is described as

$$ {}_0^C I_\tau^\alpha \left({}_0^C D_\tau^\alpha h(\tau) \right) = h(\tau) - \sum_{j=0}^{\lceil \alpha \rceil - 1} \frac{\tau^j}{\Gamma(j)} h^{(j)}(0), \quad \tau > 0. \tag{7} $$

3 Wavelets and Function Approximation

3.1 Brief Overview of Ultraspherical Wavelets

The USWs $\psi_{n,m}^{\gamma}(\tau) = \psi(k, n, m, \gamma, \tau)$ contain five arguments, where $k \in \mathbb{Z}_0^+$, $n = 1, 2, 3, \ldots, 2^k$, m be the degree of Ultraspherical polynomials such as $m = 0, 1, 2, \ldots, M-1$, $M \in \mathbb{N}$, τ be the normalized time, and γ is known as Ultraspherical parameter such that $\gamma > -\frac{1}{2}$.

The USWs are defined on $[0, 1]$ as [67–69]

$$ \psi_{n,m}^{\gamma}(\tau) = \begin{cases} 2^{\frac{k+1}{2}} \mu_{m,\gamma} \; U_m^{\gamma}\left(2^{k+1}\tau\text{-}2\text{n}+1\right), & \frac{(\text{n-1})}{2^k} \leq \tau \leq \frac{n}{2^k}, \\ 0, & elsewhere \end{cases} \tag{8} $$

where

$$ \mu_{m,\gamma} = 2^{\gamma}\Gamma(\gamma)\sqrt{\frac{\Gamma(m+1)\,(m+\gamma)}{2\pi\,\Gamma\,(m+2\gamma)}}, \tag{9} $$

and $\Gamma(.)$ denotes the Gamma function [70].

Here, $U_m^{\gamma}(\tau)$ is the Ultraspherical polynomial [67,68] defined on $[-1, 1]$ having degree m and satisfies following recurrence relations:

$$ U_0^{\gamma}(\tau) = 1, $$
$$ U_1^{\gamma}(\tau) = 2\gamma\tau, $$
$$ U_{n+1}^{\gamma}(\tau) = \frac{2\,(n+\gamma)\,\tau\,U_n^{\gamma}(\tau) - (n-1+2\gamma)\;U_{n-1}^{\gamma}(\tau)}{n+1}, \quad n = 1, 2, \ldots $$

With respect to the weighted function $w(\tau) = \left(1-\tau^2\right)^{\gamma-\frac{1}{2}}$, the aforementioned polynomials are orthogonal and the set of USWs is orthogonal on $[0, 1]$ under the weight function $w_{n,k}(\tau)$, where

$$ w_{n,k}(\tau) = w\left(2^{k+1}\tau\text{-}2\text{n}+1\right). $$

3.2 Function Approximation

Let $\left\{\psi_{1,0}^{\gamma}(\tau), \ldots, \psi_{1,M-1}^{\gamma}(\tau), \psi_{2,0}^{\gamma}(\tau), \ldots, \psi_{2,M-1}^{\gamma}(\tau), \ldots, \psi_{2^{k-1},0}^{\gamma}(\tau), \ldots, \psi_{2^{k-1},(M-1)}^{\gamma}(\tau)\right\} \in L^2[0, 1]$ is the set of USWs,

$S = Span\left\{\psi_{1,0}^{\gamma}(\tau), \ldots, \psi_{1,M-1}^{\gamma}(\tau), \psi_{2,0}^{\gamma}(\tau), \ldots, \psi_{2,M-1}^{\gamma}(\tau), \ldots, \psi_{2^{k-1},0}^{\gamma}(\tau), \ldots, \psi_{2^{k-1},(M-1)}^{\gamma}(\tau)\right\}$, and $h(\tau) \in L^2[0, 1]$ is any element. Then, from the finite-dimensional vector space S, $h(\tau)$ has the best approximation such that

$$ \|h(\tau) - h_0(\tau)\| < \|h(\tau) - f(\tau)\|; h_0(\tau), f(\tau) \in S. $$

An arbitrary function $h(\tau) \in L^2[0,1]$ may be described as a combination of USWs as

$$h(\tau) \approx \sum_{n=1}^{\infty} \sum_{m=0}^{\infty} c_{n,m} \psi_{n,m}^{\gamma}(\tau), \tag{10}$$

where $c_{n,m}$ be the unknown coefficient corresponding to $\psi_{n,m}^{\gamma}(\tau)$.

If the given series in Eq. (10) is truncated, we obtain

$$h(\tau) \approx \sum_{n=1}^{2^{k-1}} \sum_{m=0}^{M-1} c_{n,m} \psi_{n,m}^{\gamma}(\tau) = C^T \Psi_{\tilde{\sigma}}^{\gamma}(\tau), \tag{11}$$

where $\Psi_{\tilde{\sigma}}^{\gamma}(\tau)$ and C are $2^{k-1}M \times 1$ order matrices provided by

$$C^T = \left[c_{1,0}, c_{1,1}, \ldots, c_{1,M-1}, c_{2,0}, c_{2,1}, \ldots, c_{2,M-1}, \ldots, c_{2^{k-1},0}, c_{2^{k-1},1}, \ldots, c_{2^{k-1},M-1}\right], \tag{12}$$

$$\Psi_{\tilde{\sigma}}^{\gamma}(\tau) = \left[\psi_{1,0}^{\gamma}(\tau), \ldots, \psi_{1,M-1}^{\gamma}(\tau), \psi_{2,0}^{\gamma}(\tau), \ldots, \psi_{2,M-1}^{\gamma}(\tau), \ldots, \psi_{2^{k-1},0}^{\gamma}(\tau), \ldots, \psi_{2^{k-1},M-1}^{\gamma}(\tau)\right]^T. \tag{13}$$

In this study, we use $2^{k-1}M = \tilde{\sigma}$ to represent the total USWs basis in the calculating process. Any unknown function can be computed with ease utilizing the concept of function approximation corresponding to known USWs and the computational complexity is minimized in comparison to other available techniques.

4 Solution of Caputo Fractional Rössler Attractor Model

In the present section, the Caputo fractional Rössler attractor model is solved by the USWs scheme with the collocation points. In this study, we selected the specific collocation points given in Eq. (25) because they are uniformly distributed over the interval, simplifying implementation and ensuring that the computational load is evenly distributed across the domain. Uniformly distributed points are particularly well-suited for our method, as they align well with the USWs framework, preserving the accuracy of the numerical solution for the fractional Rössler attractor model.

To evaluate the solutions of the Caputo fractional Rössler attractor model, the procedure of the described wavelets scheme is given as:

4.1 For Model 1 (Asymmetric Caputo Fractional Rössler Attractor Model)

Consider the asymmetric Caputo fractional Rössler attractor model given in Eq. (1) and provide the approximation for the unknown function ${}_0^C D_\tau^\alpha x(\tau)$ of Eq. (1) as combination of USWs using Eq. (11) as

$${}_0^C D_\tau^\alpha x(\tau) \approx \sum_{n=1}^{2^{k-1}} \sum_{m=0}^{M-1} c_{n,m}^{(1)} \psi_{n,m}^{\gamma}(\tau) = {C_1}^T \Psi_{\tilde{\sigma}}^{\gamma}(\tau), \tag{14}$$

where $\Psi_{\tilde{\sigma}}^{\gamma}(\tau)$ is given in Eqs. (8) and (13) and wavelet coefficients C_1^T is defined as

$$C_1^T = \left[c_{1,0}^{(1)}, c_{1,1}^{(1)}, \ldots, c_{1,M-1}^{(1)}, c_{2,0}^{(1)}, c_{2,1}^{(1)}, \ldots, c_{2,M-1}^{(1)}, \ldots, c_{2^{k-1},0}^{(1)}, c_{2^{k-1},1}^{(1)}, \ldots, c_{2^{k-1},M-1}^{(1)}\right]. \tag{15}$$

Taking the integral of Eq. (6) on Eq. (14), and using Eqs. (2) and (7), we get

$$\begin{aligned} {}_0^C I_\tau^\alpha ({}_0^C D_\tau^\alpha x(\tau)) &= {C_1}^T \frac{1}{\Gamma(\alpha)} \int_0^\tau (\tau - t)^{\alpha-1} \Psi_{\tilde{\sigma}}^\gamma(t) dt \\ x(\tau) - x(0) &= {C_1}^T \frac{1}{\Gamma(\alpha)} \int_0^\tau (\tau - t)^{\alpha-1} \Psi_{\tilde{\sigma}}^\gamma(t) dt \\ x(\tau) &= x_1 + {C_1}^T \frac{1}{\Gamma(\alpha)} \int_0^\tau (\tau - t)^{\alpha-1} \Psi_{\tilde{\sigma}}^\gamma(t) dt \\ x(\tau) &= x_1 + {C_1}^T \frac{1}{\Gamma(\alpha)} G(\tau, \alpha, \gamma), \end{aligned} \tag{16}$$

where $G(\tau, \alpha, \gamma) = \int_0^\tau (\tau - t)^{\alpha-1} \Psi_{\tilde{\sigma}}^\gamma(t) dt$ is computed directly by performing integration in Mathematica.

Similarly, the unknown function ${}_0^C D_\tau^\alpha y(\tau)$ in Eq. (1) is expressed through USWs as

$${}_0^C D_\tau^\alpha y(\tau) \approx \sum_{n=1}^{2^{k-1}} \sum_{m=0}^{M-1} c_{n,m}^{(2)} \psi_{n,m}^\gamma(\tau) = {C_2}^T \Psi_{\tilde{\sigma}}^\gamma(\tau), \tag{17}$$

where wavelet coefficient C_2^T is defined as

$$C_2^T = \left[c_{1,0}^{(2)}, c_{1,1}^{(2)}, \ldots, c_{1,M-1}^{(2)}, c_{2,0}^{(2)}, c_{2,1}^{(2)}, \ldots, c_{2,M-1}^{(2)}, \ldots, c_{2^{k-1},0}^{(2)}, c_{2^{k-1},1}^{(2)}, \ldots, c_{2^{k-1},M-1}^{(2)} \right]. \tag{18}$$

Taking integral of Eq. (6) on Eq. (17) and using Eqs. (2) and (7), we get

$$\begin{aligned} {}_0^C I_\tau^\alpha ({}_0^C D_\tau^\alpha y(\tau)) &= {C_2}^T \frac{1}{\Gamma(\alpha)} \int_0^\tau (\tau - t)^{\alpha-1} \Psi_{\tilde{\sigma}}^\gamma(t) dt \\ y(\tau) - y(0) &= {C_2}^T \frac{1}{\Gamma(\alpha)} \int_0^\tau (\tau - t)^{\alpha-1} \Psi_{\tilde{\sigma}}^\gamma(t) dt \\ y(\tau) &= y_1 + {C_2}^T \frac{1}{\Gamma(\alpha)} G(\tau, \alpha, \gamma). \end{aligned} \tag{19}$$

Similarly, the unknown term ${}_0^C D_\tau^\alpha z(\tau)$ in Eq. (1) is expressed via UVWs as

$${}_0^C D_\tau^\alpha z(\tau) \approx \sum_{n=1}^{2^{k-1}} \sum_{m=0}^{M-1} c_{n,m}^{(3)} \psi_{n,m}^\gamma(\tau) = {C_3}^T \Psi_{\tilde{\sigma}}^\gamma(\tau), \tag{20}$$

where wavelet coefficient C_3^T is defined as

$$C_3^T = \left[c_{1,0}^{(3)}, c_{1,1}^{(3)}, \ldots, c_{1,M-1}^{(3)}, c_{2,0}^{(3)}, c_{2,1}^{(3)}, \ldots, c_{2,M-1}^{(3)}, \ldots, c_{2^{k-1},0}^{(3)}, c_{2^{k-1},1}^{(3)}, \ldots, c_{2^{k-1},M-1}^{(3)} \right]. \tag{21}$$

Taking integral of Eq. (6) on Eq. (20) and using Eqs. (2) and (7), we get

$$\begin{aligned} {}_0^C I_\tau^\alpha ({}_0^C D_\tau^\alpha z(\tau)) &= {C_3}^T \frac{1}{\Gamma(\alpha)} \int_0^\tau (\tau - t)^{\alpha-1} \Psi_{\tilde{\sigma}}^\gamma(t) dt \\ z(\tau) - z(0) &= {C_3}^T \frac{1}{\Gamma(\alpha)} \int_0^\tau (\tau - t)^{\alpha-1} \Psi_{\tilde{\sigma}}^\gamma(t) dt \\ z(\tau) &= z_1 + {C_3}^T \frac{1}{\Gamma(\alpha)} G(\tau, \alpha, \gamma). \end{aligned} \tag{22}$$

Substituting Eqs. (14)–(22) in Eq. (1), we get the wavelet approximate form of Eq. (1) as

$$\begin{aligned} C_1^T \Psi_{\tilde{\sigma}}^{\gamma}(\tau) &= -\left(y_1 + {C_2}^T \frac{1}{\Gamma(\alpha)} G(\tau,\alpha,\gamma)\right) - \left(z_1 + {C_3}^T \frac{1}{\Gamma(\alpha)} G(\tau,\alpha,\gamma)\right) \\ C_2^T \Psi_{\tilde{\sigma}}^{\gamma}(\tau) &= \left(x_1 + {C_1}^T \frac{1}{\Gamma(\alpha)} G(\tau,\alpha,\gamma)\right) + a\left(y_1 + {C_2}^T \frac{1}{\Gamma(\alpha)} G(\tau,\alpha,\gamma)\right) \\ C_3^T \Psi_{\tilde{\sigma}}^{\gamma}(\tau) &= b + \left(z_1 + {C_3}^T \frac{1}{\Gamma(\alpha)} G(\tau,\alpha,\gamma)\right)\left(\left(x_1 + {C_1}^T \frac{1}{\Gamma(\alpha)} G(\tau,\alpha,\gamma)\right) - c\right), \end{aligned} \tag{23}$$

Collocating Eq. (23) at the collocation point τ_j, $(3\tilde{\sigma})$ algebraic equations are obtained as

$$\begin{aligned} C_1^T \Psi_{\tilde{\sigma}}^{\gamma}(\tau_j) &= -\left(y_1 + {C_2}^T \frac{1}{\Gamma(\alpha)} G(\tau_j,\alpha,\gamma)\right) - \left(z_1 + {C_3}^T \frac{1}{\Gamma(\alpha)} G(\tau_j,\alpha,\gamma)\right) \\ C_2^T \Psi_{\tilde{\sigma}}^{\gamma}(\tau_j) &= \left(x_1 + {C_1}^T \frac{1}{\Gamma(\alpha)} G(\tau_j,\alpha,\gamma)\right) + a\left(y_1 + {C_2}^T \frac{1}{\Gamma(\alpha)} G(\tau_j,\alpha,\gamma)\right) \\ C_3^T \Psi_{\tilde{\sigma}}^{\gamma}(\tau_j) &= b + \left(z_1 + {C_3}^T \frac{1}{\Gamma(\alpha)} G(\tau_j,\alpha,\gamma)\right)\left(\left(x_1 + {C_1}^T \frac{1}{\Gamma(\alpha)} G(\tau_j,\alpha,\gamma)\right) - c\right), \end{aligned} \tag{24}$$

where τ_j is given by

$$\tau_j = \left(\frac{(2j-1)}{2\tilde{\sigma}}\right); \quad j = 1, 2, \ldots, \tilde{\sigma}. \tag{25}$$

Solve the system of algebraic equations in Eq. (24) by Newton iteration method, we can readily obtain the wavelet coefficient vectors C_1, C_2 and C_3. Using the value of C_1, C_2 and C_3 in Eqs. (16), (19) and (22), we estimate the wavelets approximation for $x(\tau)$, $y(\tau)$ and $z(\tau)$ of Model 1.

The algorithm of the suggested approach for Model 1 is described in Table 1.

Table 1: Algorithm of the suggested approach for Model 1

Input	$k \in \mathbb{Z}_0^+, M \in N, a, b, c, \alpha, \gamma, x_1, y_1, z_1$
Step 1	Define the USWs $\Psi_{\tilde{\sigma}}^{\gamma}(\tau)$ through Eq. (13).
Step 2	Define the 2^{k-1} M unknown vectors C_1, C_2, C_3 as Eqs. (15), (18) & (21).
Step 3	Approximate the unknown function ${}_0^C D_\tau^\alpha x(\tau)$, ${}_0^C D_\tau^\alpha y(\tau)$, ${}_0^C D_\tau^\alpha z(\tau)$ using $\Psi_{\tilde{\sigma}}^{\gamma}(\tau)$ by Eqs. (14), (17) & (20) and obtain the wavelet approximate form of Model 1 as Eq. (23).
Step 4	Introduce collocation grids τ_j as $\tau_j = \left(\frac{(2j-1)}{2\tilde{\sigma}}\right)$; $j = 1, 2, 3, \ldots, \tilde{\sigma}$.
Step 5	Generate Eq. (24) using Step 4.
Step 6	Evaluate the algebraic system attained in Step 5 and determine the vectors C_1, C_2 & C_3.
Output	Solution: $x(\tau), y(\tau), z(\tau)$

4.2 For Model 2 (Symmetric Caputo Fractional Rössler Attractor Model):

Express the unknown terms ${}_0^C D_\tau^\alpha x(\tau), {}_0^C D_\tau^\alpha y(\tau), {}_0^C D_\tau^\alpha z(\tau)$ in Eq. (3) as a combination of USWs and obtain the same Eqs. (14)–(22) using Eq. (4). Now substituting Eqs. (14)–(22) in Eq. (3), we obtain the wavelet

approximate form of Eq. (3) as

$$\begin{aligned} C_1^T \Psi_{\tilde{\sigma}}^{\gamma}(\tau) &= -\left(y_2 + {C_2}^T \frac{1}{\Gamma(\alpha)} G(\tau,\alpha,\gamma)\right) - \left(y_2 + {C_2}^T \frac{1}{\Gamma(\alpha)} G(\tau,\alpha,\gamma)\right)\left(z_2 + {C_3}^T \frac{1}{\Gamma(\alpha)} G(\tau,\alpha,\gamma)\right) \\ C_2^T \Psi_{\tilde{\sigma}}^{\gamma}(\tau) &= \left(x_2 + {C_1}^T \frac{1}{\Gamma(\alpha)} G(\tau,\alpha,\gamma)\right) + a\left(y_2 + {C_2}^T \frac{1}{\Gamma(\alpha)} G(\tau,\alpha,\gamma)\right) \\ C_3^T \Psi_{\tilde{\sigma}}^{\gamma}(\tau) &= b + \left(z_2 + {C_3}^T \frac{1}{\Gamma(\alpha)} G(\tau,\alpha,\gamma)\right)\left(\left(x_2 + {C_1}^T \frac{1}{\Gamma(\alpha)} G(\tau,\alpha,\gamma)\right)^2 - c\right). \end{aligned} \tag{26}$$

Collocating Eq. (26) at the collocation point τ_j, $(3\tilde{\sigma})$ algebraic equations are obtained as

$$\begin{aligned} C_1^T \Psi_{\tilde{\sigma}}^{\gamma}(\tau_j) &= -\left(y_2 + {C_2}^T \frac{1}{\Gamma(\alpha)} G(\tau_j,\alpha,\gamma)\right) - \left(y_2 + {C_2}^T \frac{1}{\Gamma(\alpha)} G(\tau_j,\alpha,\gamma)\right)\left(z_2 + {C_3}^T \frac{1}{\Gamma(\alpha)} G(\tau_j,\alpha,\gamma)\right) \\ C_2^T \Psi_{\tilde{\sigma}}^{\gamma}(\tau_j) &= \left(x_2 + {C_1}^T \frac{1}{\Gamma(\alpha)} G(\tau_j,\alpha,\gamma)\right) + a\left(y_2 + {C_2}^T \frac{1}{\Gamma(\alpha)} G(\tau_j,\alpha,\gamma)\right) \\ C_3^T \Psi_{\tilde{\sigma}}^{\gamma}(\tau_j) &= b + \left(z_2 + {C_3}^T \frac{1}{\Gamma(\alpha)} G(\tau_j,\alpha,\gamma)\right)\left(\left(x_2 + {C_1}^T \frac{1}{\Gamma(\alpha)} G(\tau_j,\alpha,\gamma)\right)^2 - c\right), \end{aligned} \tag{27}$$

where τ_j is provided in Eq. (25).

Evaluate the algebraic system in Eq. (27) by Newton iteration method, we can readily obtain the wavelet coefficient vectors C_1, C_2 & C_3. Using the value of C_1, C_2 & C_3, we estimate the wavelets approximation of $x(\tau)$, $y(\tau)$ & $z(\tau)$ of Model 2.

The algorithm of the proposed approach for Model 2 is described in Table 2.

Table 2: Algorithm of the suggested approach for Model 2

Input	$\boldsymbol{k \in \mathbb{Z}_0^+, M \in N, a, b, c, \alpha, \gamma, x_2, y_2, z_2}$
Step 1	Define the USWs $\Psi_{\tilde{\sigma}}^{\gamma}(\tau)$ through Eq. (13).
Step 2	Define the 2^{k-1} M unknown vectors C_1, C_2, C_3.
Step 3	Approximate the unknown function ${}_0^C D_\tau^\alpha x(\tau)$, ${}_0^C D_\tau^\alpha y(\tau)$, ${}_0^C D_\tau^\alpha z(\tau)$ using $\Psi_{\tilde{\sigma}}^{\gamma}(\tau)$ by Eqs. (14), (17) & (20) and obtained the wavelet approximate form of the Model 2 as Eq. (26).
Step 4	Introduce collocation grids τ_j as $\tau_j = \left(\frac{(2j-1)}{2\tilde{\sigma}}\right)$; $j = 1, 2, 3, \ldots, \tilde{\sigma}$.
Step 5	Generate the Eq. (26) using Step 4.
Step 6	Evaluate the algebraic system attained in Step 5 and determine the vectors C_1, C_2 & C_3.
Output	Solution $x(\tau), y(\tau), z(\tau)$

5 Error and Equilibria Analysis

This section first presents a detailed error analysis, followed by a comprehensive stability analysis of the Caputo fractional Rössler attractor model.

5.1 Error Analysis

The residual error formula is presented for comparison purposes and to examine the efficacy of the described approach. The analytical solution of the considered model is not available for integer and non-integer order, therefore we provide a residual error function to assess the precision of the given scheme.

- For asymmetric fractional Rössler attractor, the residual error function is given as

$$R_x(\tau) = \left|{}_0^C D_\tau^\alpha x_{\tilde{\sigma}}(\tau) + y_{\tilde{\sigma}}(\tau) + z_{\tilde{\sigma}}(\tau)\right|,$$
$$R_y(\tau) = \left|{}_0^C D_\tau^\alpha y_{\tilde{\sigma}}(\tau) - x_{\tilde{\sigma}}(\tau) - a y_{\tilde{\sigma}}(\tau)\right|,$$
$$R_z(\tau) = \left|{}_0^C D_\tau^\alpha z_{\tilde{\sigma}}(\tau) - b - z_{\tilde{\sigma}}(\tau)(x_{\tilde{\sigma}}(\tau) - c)\right|,$$

  where $x_{\tilde{\sigma}}(\tau)$, $y_{\tilde{\sigma}}(\tau)$ *and* $z_{\tilde{\sigma}}(\tau)$ are wavelets approximated solutions of the considered Model 1.
- For symmetric fractional Rössler attractor, the residual error function is given as

$$R_x(\tau) = \left|{}_0^C D_\tau^\alpha x_{\tilde{\sigma}}(\tau) + y_{\tilde{\sigma}}(\tau) + y_{\tilde{\sigma}}(\tau) z_{\tilde{\sigma}}(\tau)\right|,$$
$$R_y(\tau) = \left|{}_0^C D_\tau^\alpha y(\tau) - x_{\tilde{\sigma}}(\tau) - a y_{\tilde{\sigma}}(\tau)\right|,$$
$$R_z(\tau) = \left|{}_0^C D_\tau^\alpha z_{\tilde{\sigma}}(\tau) - b - z_{\tilde{\sigma}}(\tau)((x_{\tilde{\sigma}}(\tau))^2 - c)\right|.$$

- The maximum residual error ($RE_{\max}$) is calculated as

$$RE\left(x(\tau)\right)_{\max} = \max_{\tau\in[0,1]} |R_x(\tau)|,$$
$$RE\left(y(\tau)\right)_{\max} = \max_{\tau\in[0,1]} |R_y(\tau)|,$$
$$RE\left(z(\tau)\right)_{\max} = \max_{\tau\in[0,1]} |R_z(\tau)|.$$

- The minimum residual error ($RE_{\min}$) is calculated as

$$RE\left(x(\tau)\right)_{\min} = \min_{\tau\in[0,1]} |R_x(\tau)|,$$
$$RE\left(y(\tau)\right)_{\min} = \min_{\tau\in[0,1]} |R_y(\tau)|,$$
$$RE\left(z(\tau)\right)_{\min} = \min_{\tau\in[0,1]} |R_z(\tau)|.$$

- The L_2-Residual error is determined by

$$L_2\ error = \left|\left|R\left(\tau\right)\right|\right|_{\mathrm{L}^2[0,1]} = \sqrt{\int_0^1 \left(R\left(\tau\right)\right)^2 d\tau}.$$

The fundamental findings corresponding to the approximation of Ultraspherical polynomials serve as the foundation for exploring the convergence of USWs approximations. The convergence of the series expansion of $h(\tau) \in L^2[0,1]$ is given by the following theorem.

Theorem 5.1. *Consider the USWs expansion* $\sum_{n=1}^{2^{k-1}} \sum_{m=0}^{M-1} c_{n,m} \psi_{n,m}^{\gamma}(\tau) = \sum_{j=0}^{\tilde{\sigma}} c_j \psi_j^{\gamma}(\tau) = C^T \Psi_{\tilde{\sigma}}^{\gamma}(\tau)$ *of a function* $h(\tau) \in L^2[0,1]$, *the error estimate is obtained as*

$$\left\| h(\tau) - \sum_{j=0}^{\tilde{\sigma}} c_j \psi_j^{\gamma}(\tau) \right\|_2 \leq \frac{\aleph (1+\gamma)^2 (M+\gamma)}{(M-3)^{7/2} 4^k},$$

where $\aleph = \max_{\tau \in [0,1]} \left| h^{m+1}(\tau) \right|$.

Also,

$$\lim_{\tilde{\sigma} \to \infty} \left\| h(\tau) - \sum_{j=0}^{\tilde{\sigma}} c_j \psi_j^{\gamma}(\tau) \right\| = 0,$$

where $\tilde{\sigma} = 2^{k-1} M$.

Proof. For proof, see [68]. ■

5.2 Existence and Uniqueness of Solution

Theorem 5.2. *Every solution of the system (1) and (3) with positive initial values* $x(0)$, $y(0)$, $z(0)$ *exists and is unique in the interval* $[0, \infty)$.

Proof. For Model 1:

Let $\mathrm{X}^* = (x, y, z)^T$ and $G(\mathrm{X}^*) = (G_1(\mathrm{X}^*), G_2(\mathrm{X}^*), G_3(\mathrm{X}^*))^T$ such that

$$\begin{aligned} G_1(\mathrm{X}^*) &= -y(\tau) - z(\tau) = 0, \\ G_2(\mathrm{X}^*) &= x(\tau) + ay(\tau) = 0, \\ G_3(\mathrm{X}^*) &= b + z(\tau)(x(\tau) - c) = 0. \end{aligned} \tag{28}$$

Therefore, the system in (28) can be written in the form $\hat{\mathrm{X}}^* = G(\mathrm{X}^*)$ where $G(\mathrm{X}^*) : \mathbb{R}_+ \to \mathbb{R}_+^3$ with $\mathrm{X}^*(0) = \mathrm{X}_0^* \in \mathbb{R}_+^3$, $G_r \in \mathbb{R}^{\infty}\left(\mathbb{R}_+^3\right)$ for $r = 1, 2, 3$. Consequently, the vector function G is a fully continuous and locally Lipschitzian function of the variables x, y & z in the positive quadrant $W = \{(x(\tau), y(\tau), z(\tau)); x > 0, y > 0, z > 0\}$. As a result, we can easily state that any solution (x, y, z) to system (1) with positive initial values exists and is unique across the interval $[0, \infty)$ for all $\tau \geq 0$.

For Model 2: Same proof as above. ■

5.3 Equilibria Analysis

The solution of the Caputo fractional Rössler attractor model is overall assessed on the groundwork of steadiness points [64,65]. The steadiness points of the regarded model are attained by resolving the model under uniform state conditions. The examination of equilibrium points is split up into the eigenvalues signs. The Jacobian matrix of the model is constructed to analyze the signs of the eigenvalues to determine stability. Then, the behavior of the considered fractional model for each point of equilibrium can be subjectively evaluated by inspecting the nature of eigenvalues. When the Jacobian matrix has complex eigenvalues and the real part of the eigenvalues corresponding to the equilibrium points is positive, then the equilibrium points are the saddle spiral points. Also, if the Jacobian matrix has complex eigenvalues and positive real eigenvalues corresponding to the equilibrium points, then the equilibrium points are also saddle spiral points. The equilibrium points of the considered system will be asymptotically stable if all eigenvalues of the associated

Jacobian matrix fulfill the Matignon condition [71]. The particular values of the parameters involved in the considered model are taken from [58].

For Model 1: The equilibrium points for asymmetric Caputo fractional Rössler attractor model are obtained as

$${}_0^C D_\tau^\alpha x(\tau) = 0,\ {}_0^C D_\tau^\alpha y(\tau) = 0, {}_0^C D_\tau^\alpha z(\tau) = 0,$$

i.e.,

$$\begin{aligned} -y(\tau) - z(\tau) &= 0, \\ x(\tau) + a y(\tau) &= 0, \\ b + z(\tau)(x(\tau) - c) &= 0. \end{aligned} \tag{29}$$

The equilibrium points (E_i) of Eq. (1) are determined by solving Eq. (29) as

$$(\mathrm{E}_1, \mathrm{E}_2) = \left((a\beta_1, -\beta_1, \beta_1), (a\beta_2, -\beta_2, \beta_2)\right),$$

where

$$\beta_1 = \frac{1}{2}\left(\frac{c - \sqrt{c^2 - 4ab}}{a}\right),$$
$$\beta_2 = \frac{1}{2}\left(\frac{c + \sqrt{c^2 - 4ab}}{a}\right).$$

Computing Jacobian Matrix$J$ for the considered Model 1 as

$$J = \begin{pmatrix} 0 & -1 & -1 \\ 1 & a & 0 \\ z & 0 & -c + x \end{pmatrix}. \tag{30}$$

- The Jacobian Matrix at E_1 using Eq. (30) is given as

$$J(\mathrm{E}_1) = \begin{pmatrix} 0 & -1 & -1 \\ 1 & a & 0 \\ \left(\frac{1}{2}\left(\frac{c - \sqrt{c^2 - 4ab}}{a}\right)\right) & 0 & -c + a\left(\frac{1}{2}\left(\frac{c - \sqrt{c^2 - 4ab}}{a}\right)\right) \end{pmatrix}.$$

The eigenvalues of $J(E_1)$ are computed by finding the roots of its characteristic equation as the form of $(-\Upsilon_1 - \eta_1 \boldsymbol{i}, -\Upsilon_1 + \eta_1 \boldsymbol{i}, \boldsymbol{\kappa_1})$, where Υ_1 represents real part and η_1 represents imaginary part, and κ_1 represents the real number.

For $a = 0.2, b = 0.2, c = 5.7$, the eigenvalues are obtained as:
$\left(-4.59607 \times 10^{-6} - 5.42803\, i, -4.59607 \times 10^{-6} + 5.42803\, i, 0.192983\right)$.

- The Jacobian Matrix at E_2 using Eq. (30) is given as

$$J(\mathrm{E}_2) = \begin{pmatrix} 0 & -1 & -1 \\ 1 & a & 0 \\ \frac{1}{2}\left(\frac{c + \sqrt{c^2 - 4ab}}{a}\right) & 0 & -c + a\left(\frac{1}{2}\left(\frac{c + \sqrt{c^2 - 4ab}}{a}\right)\right) \end{pmatrix}.$$

The eigenvalues of $J(E_2)$ are computed by finding the roots of its characteristic equation as the form of $(\Upsilon_2 - \eta_2 \boldsymbol{i}, \Upsilon_2 + \eta_2 \boldsymbol{i}, -\boldsymbol{\kappa}_2)$, where Υ_2 represents real part and η_2 represents imaginary part, and κ_2 represents the real number.

For $a = 0.2, b = 0.2, c = 5.7$, the eigenvalues are obtained as:

$\left(9.70009 \times 10^{-2} - 9.95193 \times 10^{-1}\, i,\ 9.70009 \times 10^{-2} + 9.95193 \times 10^{-1}\, i,\ -5.6869\right)$.

The discriminant of the characteristic equation of the Jacobian matrix corresponding to the equilibrium points E_1 & E_2 for Model 1 is less than zero under the assumed value of the model's parameters, therefore we obtained two imaginary roots and one real root for $J(E_1)$ & $J(E_2)$. It is observed from general and particular values of eigenvalues, E_1 & E_2 are spiral saddle points for Model 1.

For Model 2: The equilibrium points for symmetric Caputo fractional Rössler attractor model are obtained as

$${}_0^C D_\tau^\alpha x(\tau) = 0,\ {}_0^C D_\tau^\alpha y(\tau) = 0, {}_0^C D_\tau^\alpha z(\tau) = 0,$$

i.e.,

$$\begin{aligned} -y(\tau) - y(\tau)z(\tau) &= 0, \\ x(\tau) + ay(\tau) &= 0, \\ b + z(\tau)((x(\tau))^2 - c) &= 0. \end{aligned} \tag{31}$$

By solving Eq. (31), we get the model's equilibrium points.

The equilibrium points (E_i) of Eq. (3) are obtained by solving Eq. (31) as

$$(E_1, E_2, E_3) = \left(\left(0, 0, \frac{b}{c}\right), (-a\rho, \rho, -1), (a\rho, -\rho, -1)\right),$$

where $\rho = \sqrt{\frac{b+c}{a^2}}$.

Computing Jacobian Matrix J for the considered model as

$$J = \begin{pmatrix} 0 & -1 - z & -y \\ 1 & a & 0 \\ 2xz & 0 & -c + x^2 \end{pmatrix}. \tag{32}$$

- The Jacobian Matrix at E_1 using Eq. (32) is given as

$$J(E_1) = \begin{pmatrix} 0 & -1 - \dfrac{b}{c} & 0 \\ 1 & a & 0 \\ 0 & 0 & -c \end{pmatrix}.$$

The eigenvalues for $J(E_1)$ are computed by finding the roots of its characteristic equation as $\left(\frac{(a - \mathbf{D}_1 i)}{2}, \frac{(a + \mathbf{D}_1 i)}{2}, -c\right)$, where $\mathbf{D}_1$ represents real number.

For $a = 0.4, b = 0.4, c = 4.5$, the eigenvalues are obtained as: $(0.2 - 1.02415\, i, 0.2 + 1.02415\, i, -4.5)$.

- The Jacobian Matrix at E_2 using Eq. (32) is given as

$$J(\mathrm{E}_2) = \begin{pmatrix} 0 & 0 & -\dfrac{\sqrt{b+c}}{a} \\ 1 & a & 0 \\ 2\sqrt{b+c} & 0 & b \end{pmatrix}.$$

The eigenvalues for $J(E_2)$ are computed by finding the roots of its characteristic equation as $\left(\frac{(b+\mathbf{D}_2 i)}{2}, \frac{(b-\mathbf{D}_2 i)}{2}, a\right)$.

For $a = 0.4, b = 0.4, c = 4.5$, the eigenvalues are obtained as: $(0.2 + 4.9457\, i,\ 0.2 - 4.9457\, i,\ 0.4)$.

- The Jacobian Matrix at E_3 using Eq. (32) is given as

$$J(\mathrm{E}_3) = \begin{pmatrix} 0 & 0 & \dfrac{\sqrt{b+c}}{a} \\ 1 & a & 0 \\ -2\sqrt{b+c} & 0 & b \end{pmatrix}.$$

The eigenvalues for $J(E_3)$ are computed by finding the roots of its characteristic equation as $\left(\frac{(b+\mathbf{D}_2 i)}{2}, \frac{(b-\mathbf{D}_2 i)}{2}, a\right)$.

For $a = 0.4, b = 0.4, c = 4.5$, the eigenvalues are are obtained as: $(0.2 + 4.94571\, i,\ 0.2 - 4.94571\, i,\ 0.4)$.

The discriminant of the characteristic equation of the Jacobian matrix corresponding to the equilibrium points E_1, E_2 & E_3 for Model 2 is also less than zero under the assumed value of the model's parameters, therefore we obtained two imaginary roots and one real root for $J(E_1)$, $J(E_2)$ & $J(E_3)$. It is observed from the general and particular values of eigenvalues, E_1, E_2 & E_3 are spiral saddle points for Model 2.

6 Numerical Simulations and Discussion

The effectiveness and performance of the suggested approach are assessed by employing it in several cases, and the results are contrasted with existing systems that offer accurate solutions. In this study, both maximum and minimum residual errors are computed. Mentioning both residual errors provides a comprehensive view of model performance, and a clear range of errors, and allows for better assessment and comparison. All numerical results are obtained using Mathematica. All codes and figures in this study are executed and generated on the following kind of machine: Windows 10 Home operating system (64-bit), RAM of 8 GB, Intel Core i5-8250U CPU @ 1.60 GHz.

Now, both Caputo fractional Rössler attractor models are simulated for particular parameters [58] and their impact on the dynamics of the Caputo fractional Rössler attractor model.

6.1 Asymmetric Caputo Fractional Rössler Attractor Model

The asymmetric Caputo fractional Rössler attractor model is numerically simulated for $a = 0.2$, $b = 0.2$, $c = 5.7$ and the initial conditions $x_1 = 1$, $y_1 = 1$, $z_1 = 1.05$.

For this case, the Rössler model is represented through the following equations as

$$\begin{aligned} {}_0^C D_\tau^\alpha x(\tau) &= -y(\tau) - z(\tau), \\ {}_0^C D_\tau^\alpha y(\tau) &= x(\tau) + a y(\tau), \\ {}_0^C D_\tau^\alpha z(\tau) &= b + z(\tau)(x(\tau) - c), \end{aligned}$$

with the conditions

$$(x_1, y_1, z_1) = (1, 1, 1.05)\,.$$

Since there is no solution and no comparison available for integer and non-integer order of this model, therefore we simulated this model for different α by the mentioned approach for $\tilde{\sigma} = 6$, and the approximate solutions are obtained as:

At $\alpha = 1$,

$$\begin{aligned}
x(\tau) &= 0.999 - 2.047\tau + 1.739\tau^2 - 2.935\tau^3 + 2.683\tau^4 - 1.308\tau^5 + 0.283\tau^6,\\
y(\tau) &= 1. + 1.199\tau - 0.893\tau^2 + 0.467\tau^3 - 0.575\tau^4 + 0.325\tau^5 - 0.0729\tau^6,\\
z(\tau) &= 1.049 - 4.743\tau + 10.189\tau^2 - 12.881\tau^3 + 10.043\tau^4 - 4.5277\tau^5 + 0.907\tau^6.
\end{aligned}$$

At $\alpha = 0.9$,

$$\begin{aligned}
x(\tau) &= 1.0 - 2.076\tau^{0.9} + 1.965\tau^{1.9} - 4.255\tau^{2.9} + 5.063\tau^{3.9} - 3.139\tau^{4.9} + 0.8204\tau^{5.9},\\
y(\tau) &= 1.0 + 1.226\tau^{0.9} - 1.1623\tau^{1.9} + 0.879\tau^{2.9} - 1.1674\tau^{3.9} + 0.787\tau^{4.9} - 0.21001\tau^{5.9},\\
z(\tau) &= 1.05 - 4.681\tau^{0.9} + 12.38\tau^{1.9} - 21.474\tau^{2.9} + 23.409\tau^{3.9} - 14.385\tau^{4.9} + 3.7609\tau^{5.9}.
\end{aligned}$$

At $\alpha = 0.8$,

$$\begin{aligned}
x(\tau) &= 1.0 - 2.0684\tau^{0.8} + 1.9201\tau^{1.8} - 4.854\tau^{2.8} + 6.708\tau^{3.8} - 4.645\tau^{4.8} + 1.311\tau^{5.8},\\
y(\tau) &= 0.999 + 1.234\tau^{0.8} - 1.454\tau^{1.8} + 1.291\tau^{2.8} - 1.711\tau^{3.8} + 1.239\tau^{4.8} - 0.353\tau^{5.8},\\
z(\tau) &= 1.05 - 4.42705\tau^{0.8} + 13.423\tau^{1.8} - 27.831\tau^{2.8} + 35.103\tau^{3.8} - 24.025\tau^{4.8} + 6.793\tau^{5.8}.
\end{aligned}$$

At $\alpha = 0.7$,

$$\begin{aligned}
x(\tau) &= 1. - 2.033\tau^{0.7} + 1.625\tau^{1.7} - 4.4809\tau^{2.7} + 6.9406\tau^{3.7} - 5.2009\tau^{4.7} + 1.5496\tau^{5.7},\\
y(\tau) &= 0.999 + +1.219\tau^{0.7} - 1.792\tau^{1.7} + 1.775\tau^{2.7} - 2.213\tau^{3.7} + 1.629\tau^{4.7} - 0.4805\tau^{5.7},\\
z(\tau) &= 1.05 - 4.014\tau^{0.7} + 13.134\tau^{1.7} - 30.422\tau^{2.7} + 41.753\tau^{3.7} - 30.378\tau^{4.7} + 8.986\tau^{5.7}.
\end{aligned}$$

The estimated residual errors in the solution of asymmetric Caputo fractional Rössler attractor model for various values of α are listed in Tables 3–6, representing maximum and minimum residual errors and L_2 errors. Since no comparisons and exact solutions are available for the considered fractional model, then we have simulated it at different fractional order values and obtained the errors for different numbers of wavelet basis. Also, we have solved the considered model by using the proposed method and the fourth-order Range-Kutta method [72] for integer order. Fig. 1 provides a graphical description of the approximated solutions using the suggested approach and the fourth-order Range-Kutta method for $\alpha = 1$ and $\tilde{\sigma} = 4$, demonstrating the good consistency between them. Fig. 2 represents the wavelet approximate solutions of asymmetric Caputo fractional Rössler attractor model for different α. The plot of residual errors for Model 1 is depicted in Figs. 3–5 for different bases. When the exact solution is not available, the accuracy of the mentioned technique is demonstrated by employing the given residual error formula. The provided findings in Tables 3–6 and Figs. 3–5 also clearly show that a reduction in errors occurs when the number of USWs basis is increased.

Table 3: Estimated residual errors for Model 1 at $\alpha = 1$

τ	$x(\tau)$			$y(\tau)$			$z(\tau)$		
	$\tilde{\sigma} = 2$	$\tilde{\sigma} = 4$	$\tilde{\sigma} = 6$	$\tilde{\sigma} = 2$	$\tilde{\sigma} = 4$	$\tilde{\sigma} = 6$	$\tilde{\sigma} = 2$	$\tilde{\sigma} = 4$	$\tilde{\sigma} = 6$
0.2	3.6×10^{-2}	1.5×10^{-2}	1.3×10^{-3}	7.6×10^{-3}	3.6×10^{-3}	3.8×10^{-4}	2.8×10^{-1}	6.8×10^{-2}	5.4×10^{-3}
0.4	6.6×10^{-2}	2.8×10^{-3}	1.5×10^{-4}	1.2×10^{-2}	6.2×10^{-4}	4.0×10^{-5}	5.5×10^{-1}	1.3×10^{-2}	6.5×10^{-4}
0.6	6.4×10^{-2}	2.6×10^{-3}	1.3×10^{-4}	1.0×10^{-2}	5.7×10^{-4}	3.5×10^{-5}	5.0×10^{-1}	1.3×10^{-2}	6.3×10^{-4}
0.8	3.3×10^{-2}	1.3×10^{-2}	9.2×10^{-4}	5.1×10^{-3}	2.7×10^{-3}	2.3×10^{-4}	3.0×10^{-1}	6.8×10^{-2}	4.5×10^{-3}
1.0	2.2×10^{-1}	8.6×10^{-2}	1.6×10^{-2}	3.2×10^{-2}	1.8×10^{-2}	3.9×10^{-3}	2.1×10^{-0}	4.7×10^{-1}	8.2×10^{-2}
$RE_{\max}$	2.8×10^{-1}	1.4×10^{-1}	5.2×10^{-2}	8.2×10^{-2}	4.3×10^{-2}	1.9×10^{-2}	2.1×10^{-0}	6.3×10^{-1}	2.3×10^{-1}
$RE_{\min}$	2.2×10^{-16}	2.2×10^{-7}	1.7×10^{-6}	0.0	9.0×10^{-8}	1.7×10^{-8}	1.7×10^{-7}	2.4×10^{-6}	2.3×10^{-12}
L_2	1.0×10^{-1}	2.8×10^{-2}	6.3×10^{-3}	2.1×10^{-2}	7.2×10^{-3}	2.1×10^{-3}	8.4×10^{-1}	1.3×10^{-1}	2.7×10^{-2}

Table 4: Estimated residual errors for Model 1 at $\alpha = 0.9$

τ	$x(\tau)$			$y(\tau)$			$z(\tau)$		
	$\tilde{\sigma} = 2$	$\tilde{\sigma} = 4$	$\tilde{\sigma} = 6$	$\tilde{\sigma} = 2$	$\tilde{\sigma} = 4$	$\tilde{\sigma} = 6$	$\tilde{\sigma} = 2$	$\tilde{\sigma} = 4$	$\tilde{\sigma} = 6$
0.2	4.0×10^{-2}	9.5×10^{-3}	1.5×10^{-4}	1.5×10^{-3}	2.1×10^{-3}	5.1×10^{-5}	2.6×10^{-1}	3.3×10^{-2}	1.7×10^{-4}
0.4	7.7×10^{-2}	1.8×10^{-3}	2.1×10^{-5}	2.9×10^{-3}	4.2×10^{-4}	7.0×10^{-6}	5.4×10^{-1}	7.3×10^{-3}	4.9×10^{-6}
0.6	7.7×10^{-2}	1.8×10^{-3}	2.1×10^{-5}	2.9×10^{-3}	4.2×10^{-4}	7.0×10^{-6}	5.8×10^{-1}	8.0×10^{-3}	2.5×10^{-5}
0.8	4.0×10^{-2}	9.5×10^{-3}	1.5×10^{-4}	1.5×10^{-3}	2.1×10^{-3}	5.1×10^{-5}	3.2×10^{-1}	4.4×10^{-2}	2.9×10^{-4}
1.0	2.7×10^{-1}	6.5×10^{-2}	2.9×10^{-3}	1.0×10^{-2}	1.4×10^{-2}	9.3×10^{-4}	2.3×10^{-0}	3.2×10^{-1}	7.0×10^{-3}
$RE_{\max}$	2.7×10^{-1}	6.5×10^{-2}	2.9×10^{-3}	1.0×10^{-2}	1.4×10^{-2}	9.3×10^{-4}	2.3×10^{-0}	3.2×10^{-1}	8.7×10^{-3}
$RE_{\min}$	9.9×10^{-9}	1.8×10^{-7}	2.4×10^{-3}	9.9×10^{-9}	7.1×10^{-8}	2.6×10^{-8}	6.6×10^{-7}	1.2×10^{-6}	5.2×10^{-6}
L_2	1.1×10^{-1}	1.6×10^{-2}	5.7×10^{-4}	4.3×10^{-3}	3.8×10^{-3}	1.8×10^{-4}	8.4×10^{-1}	6.9×10^{-2}	1.4×10^{-3}

Table 5: Estimated residual errors for Model 1 at $\alpha = 0.8$

τ	$x(\tau)$			$y(\tau)$			$z(\tau)$		
	$\tilde{\sigma} = 2$	$\tilde{\sigma} = 4$	$\tilde{\sigma} = 6$	$\tilde{\sigma} = 2$	$\tilde{\sigma} = 4$	$\tilde{\sigma} = 6$	$\tilde{\sigma} = 2$	$\tilde{\sigma} = 4$	$\tilde{\sigma} = 6$
0.2	3.2×10^{-2}	1.9×10^{-2}	2.7×10^{-3}	1.4×10^{-2}	4.8×10^{-3}	7.7×10^{-4}	2.8×10^{-1}	9.8×10^{-2}	1.3×10^{-2}
0.4	5.6×10^{-2}	3.3×10^{-3}	2.9×10^{-4}	2.2×10^{-2}	7.4×10^{-4}	7.8×10^{-5}	5.3×10^{-1}	1.7×10^{-2}	1.5×10^{-3}
0.6	5.2×10^{-2}	3.0×10^{-3}	2.6×10^{-4}	1.0×10^{-2}	6.4×10^{-4}	6.5×10^{-5}	5.3×10^{-1}	1.6×10^{-2}	1.3×10^{-3}
0.8	2.6×10^{-2}	1.4×10^{-2}	1.7×10^{-3}	9.2×10^{-3}	2.9×10^{-3}	4.2×10^{-4}	2.8×10^{-1}	8.3×10^{-2}	9.5×10^{-3}
1.0	1.7×10^{-1}	9.4×10^{-2}	2.9×10^{-2}	5.7×10^{-2}	1.8×10^{-2}	6.9×10^{-3}	1.9×10^{0}	5.6×10^{-1}	1.6×10^{-1}
$RE_{\max}$	2.9×10^{-1}	2.2×10^{-1}	1.2×10^{-1}	1.7×10^{-1}	8.0×10^{-2}	4.9×10^{-2}	2.3×10^{-0}	1.1×10^{-0}	6.1×10^{-1}
$RE_{\min}$	4.4×10^{-16}	9.9×10^{-8}	1.1×10^{-6}	2.7×10^{-17}	2.5×10^{-8}	1.6×10^{-13}	8.3×10^{-7}	2.7×10^{-7}	1.8×10^{-5}
L_2	$8.\ 9 \times 10^{-2}$	3.8×10^{-2}	1.3×10^{-2}	4.1×10^{-2}	1.1×10^{-2}	5.0×10^{-3}	8.2×10^{-1}	1.9×10^{-1}	6.8×10^{-2}

Table 6: Estimated residual errors for Model 1 at $\alpha = 0.7$

τ	$x(\tau)$			$y(\tau)$			$z(\tau)$		
	$\tilde{\sigma} = 2$	$\tilde{\sigma} = 4$	$\tilde{\sigma} = 6$	$\tilde{\sigma} = 2$	$\tilde{\sigma} = 4$	$\tilde{\sigma} = 6$	$\tilde{\sigma} = 2$	$\tilde{\sigma} = 4$	$\tilde{\sigma} = 6$
0.2	2.8×10^{-2}	2.0×10^{-2}	3.8×10^{-3}	2.1×10^{-2}	5.7×10^{-3}	1.1×10^{-3}	2.8×10^{-1}	1.1×10^{-1}	2.0×10^{-2}
0.4	4.6×10^{-2}	3.3×10^{-3}	4.0×10^{-4}	3.3×10^{-2}	8.0×10^{-4}	1.0×10^{-4}	5.0×10^{-1}	1.9×10^{-2}	2.2×10^{-3}
0.6	4.1×10^{-2}	2.9×10^{-3}	3.4×10^{-4}	2.8×10^{-2}	6.5×10^{-4}	8.8×10^{-5}	4.8×10^{-1}	1.8×10^{-2}	2.0×10^{-3}
0.8	2.0×10^{-2}	1.4×10^{-2}	2.2×10^{-3}	1.3×10^{-2}	2.8×10^{-3}	5.4×10^{-4}	2.4×10^{-1}	8.8×10^{-2}	1.3×10^{-2}
1.0	1.3×10^{-1}	8.9×10^{-2}	3.7×10^{-2}	8.1×10^{-2}	1.7×10^{-2}	8.8×10^{-3}	1.6×10^{0}	5.7×10^{-1}	2.3×10^{-1}
$RE_{\max}$	3.1×10^{-1}	2.8×10^{-1}	2.0×10^{-1}	2.9×10^{-1}	1.2×10^{-1}	9.2×10^{-2}	2.6×10^{0}	1.6×10^{-0}	1.0×10^{-0}
$RE_{\min}$	2.2×10^{-16}	1.1×10^{-7}	3.8×10^{-6}	5.5×10^{-17}	1.9×10^{-7}	7.0×10^{-13}	2.6×10^{-6}	1.9×10^{-7}	5.4×10^{-7}
L_2	7.9×10^{-2}	4.3×10^{-2}	2.1×10^{-2}	6.4×10^{-2}	1.5×10^{-2}	8.5×10^{-3}	7.8×10^{-1}	2.4×10^{-1}	1.1×10^{-1}

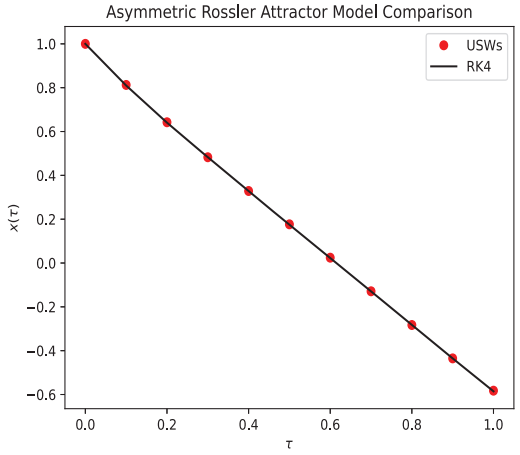

(a) $x(\tau)$

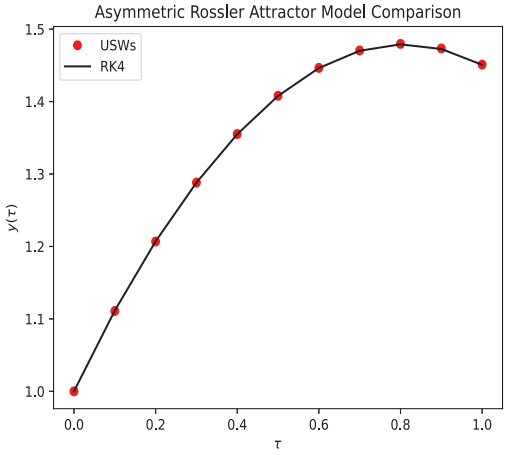

(b) $y(\tau)$

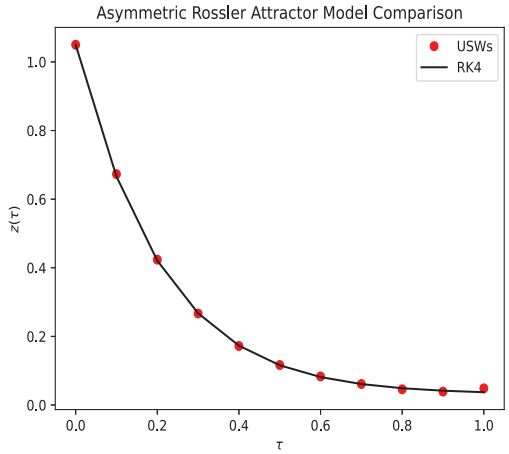

(c) $z(\tau)$

Figure 1: Solution of Model 1 via the suggested approach with fourth-order Range-Kutta method at $\alpha = 1$ & $\tilde{\sigma} = 4$

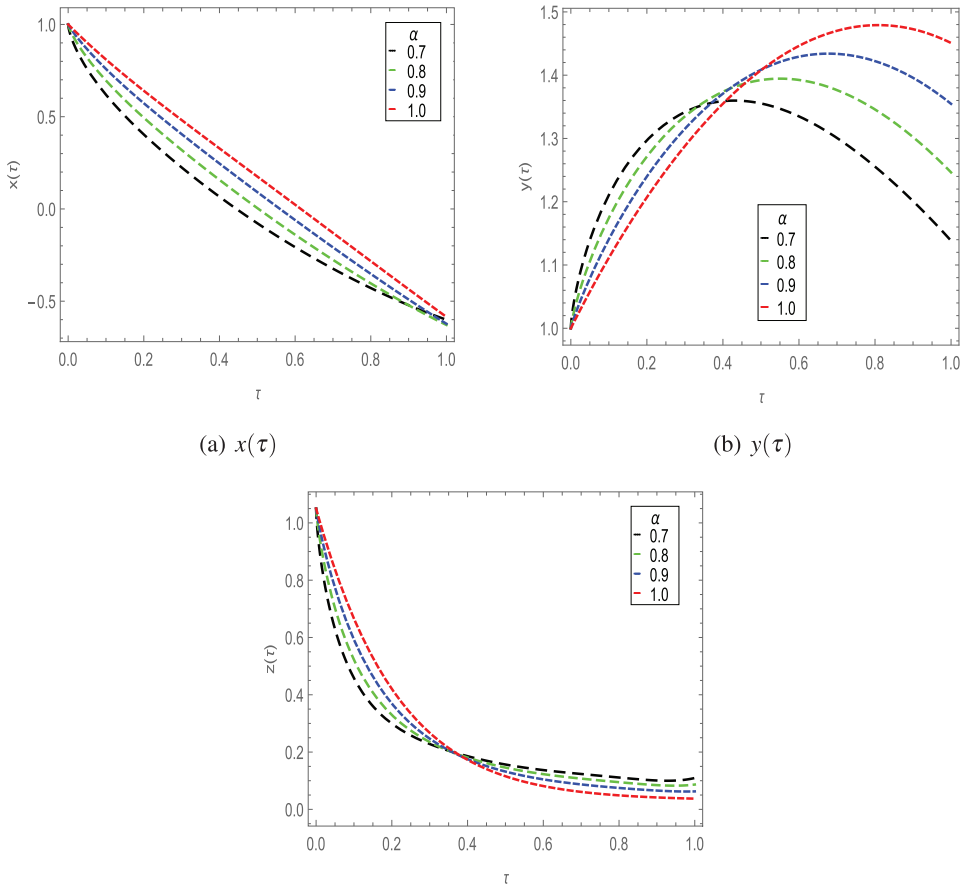

(a) $x(\tau)$ (b) $y(\tau)$

(c) $z(\tau)$

Figure 2: Solution of Model 1 for different α and $\tilde{\sigma} = 6$

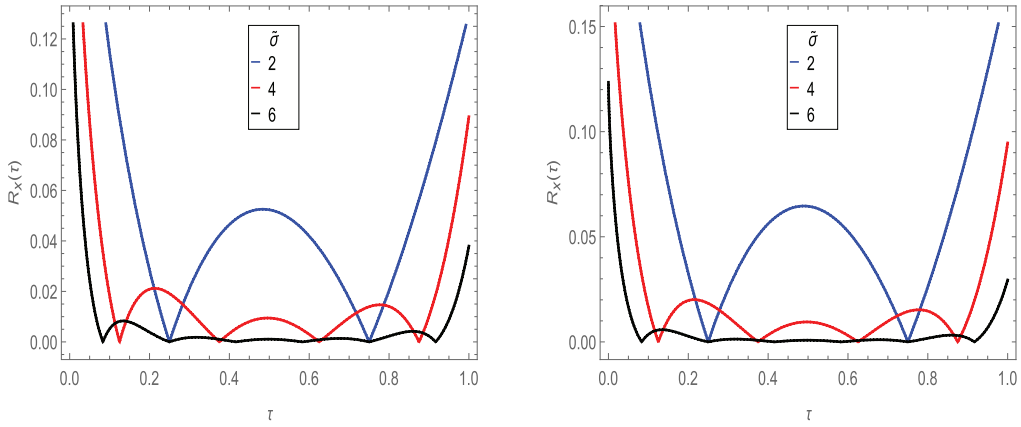

(a) $\alpha = 0.7$ (b) $\alpha = 0.8$

Figure 3: (Continued)

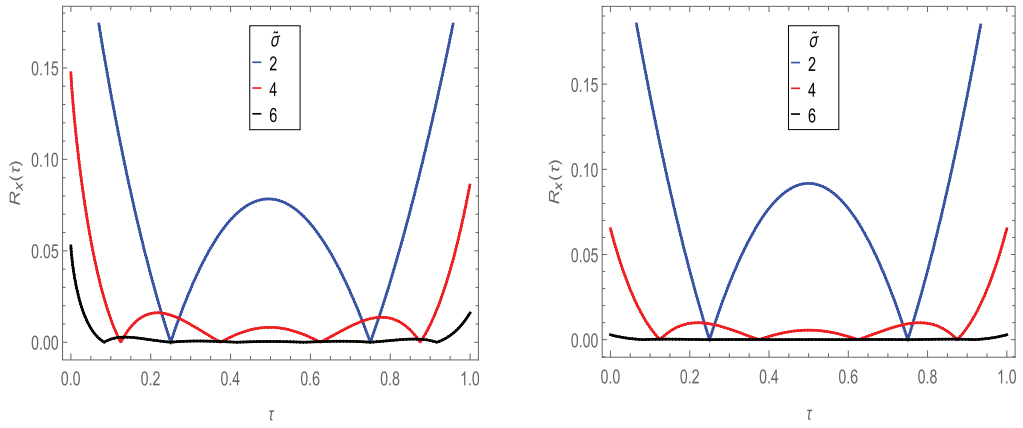

(c) $\alpha = 0.9$ (d) $\alpha = 1.0$

Figure 3: Residual error in $x(\tau)$ of Model 1 for different α and $\tilde{\sigma}$

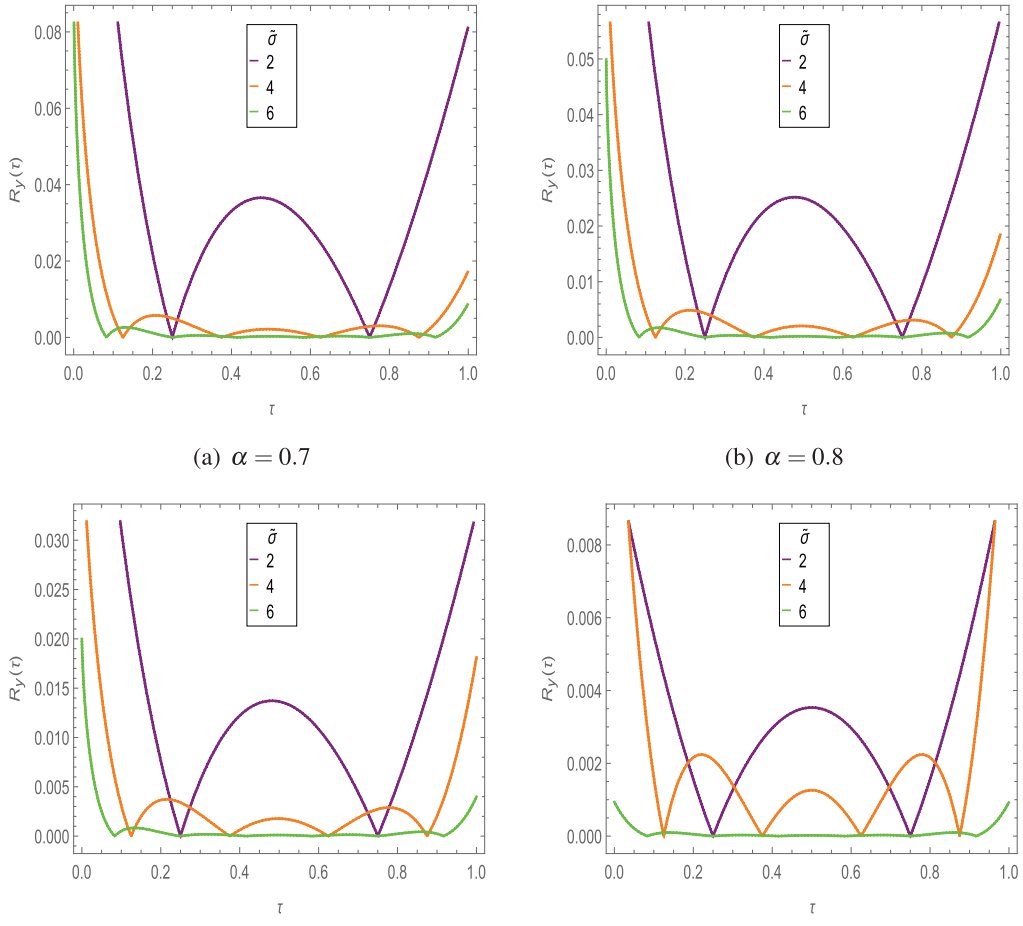

(a) $\alpha = 0.7$ (b) $\alpha = 0.8$

(c) $\alpha = 0.9$ (d) $\alpha = 1.0$

Figure 4: Residual error in $y(\tau)$ of Model 1 for different α and $\tilde{\sigma}$

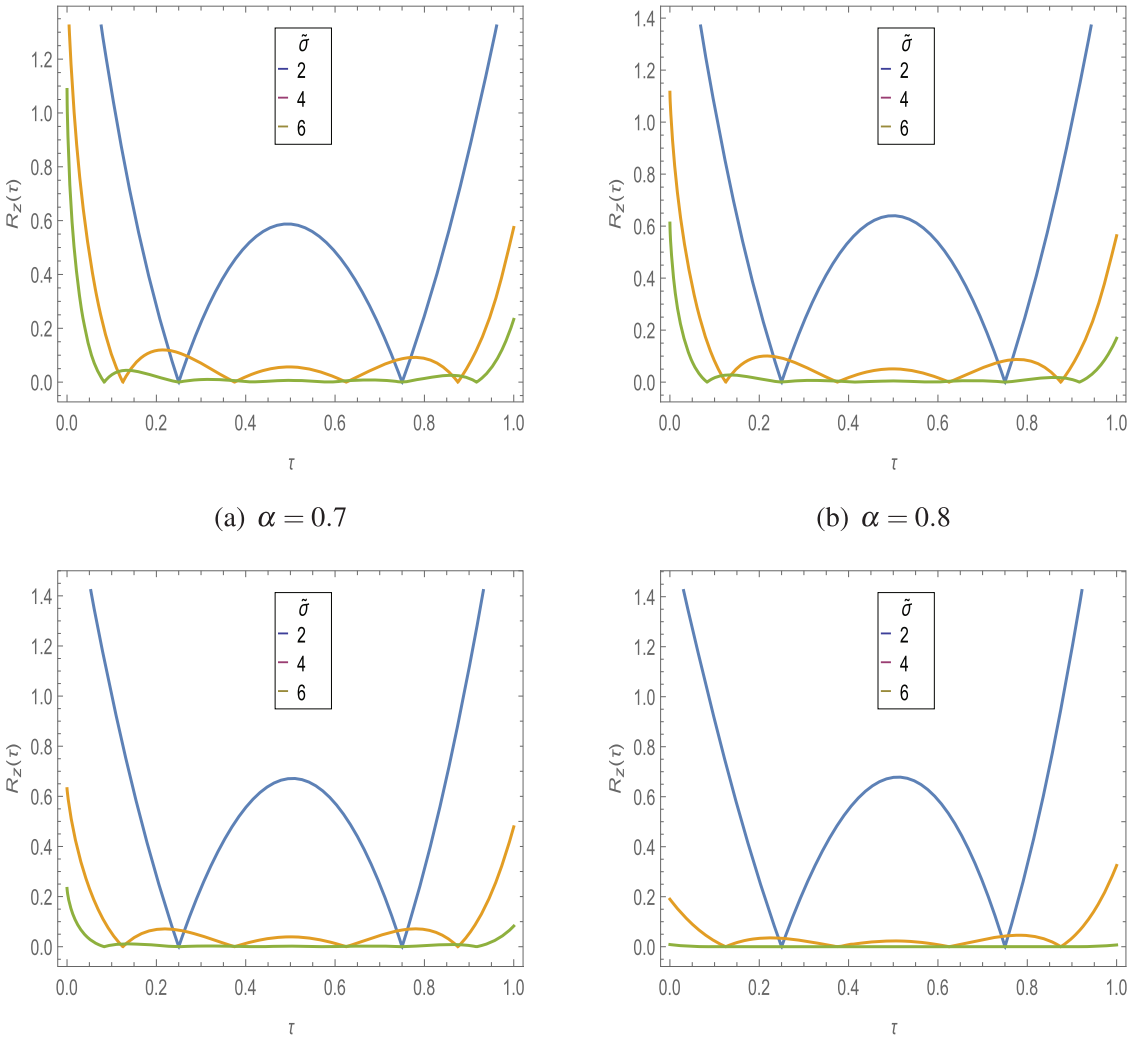

(a) $\alpha = 0.7$ (b) $\alpha = 0.8$

(c) $\alpha = 0.9$ (d) $\alpha = 1.0$

Figure 5: Residual error in $z(\tau)$ of Model 1 for different α and $\tilde{\sigma}$

6.2 Symmetric Caputo Fractional Rössler Attractor Model

The symmetric Caputo fractional Rössler attractor model is numerically simulated for $a = 0.4$, $b = 0.4$, $c = 4.5$ and the initial conditions $x(0) = 1.5$, $y(0) = 0$, $z(0) = 0$.

For this case, the Rössler model is represented through the following equations as

$$
\begin{aligned}
{}_0^C D_\tau^\alpha x(\tau) &= -y(\tau) - y(\tau)z(\tau), \\
{}_0^C D_\tau^\alpha y(\tau) &= x(\tau) + ay(\tau), \\
{}_0^C D_\tau^\alpha z(\tau) &= b + z(\tau)(x(\tau)^2 - c),
\end{aligned}
$$

with the conditions

$$(x_2, y_2, z_2) = (1.5, 0, 0).$$

Since there is no solution and no comparison available for integer and non-integer order of this model, therefore we simulated this model for different α by the mentioned approach for $\tilde{\sigma} = 6$, and the approximate solutions are obtained as:

At $\alpha = 1$,

$$x(\tau) = 1.5 + 0.0001\tau - 0.751\tau^2 - 0.287\tau^3 + 0.144\tau^4 + 0.058\tau^5 - 0.033\tau^6,$$
$$y(\tau) = \tau\left(1.5001 + 0.298\tau - 0.203\tau^2 - 0.109\tau^3 + 0.044\tau^4 - 0.0047\tau^5\right),$$
$$z(\tau) = \tau\left(0.4003 - 0.454\tau + 0.362\tau^2 - 0.483\tau^3 + 0.407\tau^4 - 0.122\tau^5\right).$$

At $\alpha = 0.9$,

$$x(\tau) = 1.5 - 0.012\tau^{0.9} - 1.077\tau^{1.9} - 0.076\tau^{2.9} + 0.141\tau^{3.9} + 0.051\tau^{4.9} - 0.038\tau^{5.9},$$
$$y(\tau) = 1.565\tau^{0.9} + 0.4008\tau^{1.9} - 0.529\tau^{2.9} + 0.105\tau^{3.9} - 0.041\tau^{4.9} + 0.014\tau^{5.9},$$
$$z(\tau) = 0.404\tau^{0.9} - 0.5608\tau^{1.9} + 0.525\tau^{2.9} - 0.639\tau^{3.9} + 0.551\tau^{4.9} - 0.182\tau^{5.9}.$$

At $\alpha = 0.8$,

$$x(\tau) = 1.5 - 0.0352\tau^{0.8} - 1.523\tau^{1.8} + 0.449\tau^{2.8} - 0.0902\tau^{3.8} + 0.109\tau^{4.8} - 0.045\tau^{5.8},$$
$$y(\tau) = 1.627\tau^{0.8} + 0.497\tau^{1.8} - 1.043\tau^{2.8} + 0.602\tau^{3.8} - 0.296\tau^{4.8} + 0.076\tau^{5.8},$$
$$z(\tau) = 0.399\tau^{0.8} - 0.6603\tau^{1.8} + 0.659\tau^{2.8} - 0.621\tau^{3.8} + 0.472\tau^{4.8} - 0.158\tau^{5.8}.$$

At $\alpha = 0.7$,

$$x(\tau) = 1.5 + 0.075\tau^{0.7} - 2.116\tau^{1.7} + 1.574\tau^{2.7} - 1.054\tau^{3.7} + 0.607\tau^{4.7} - 0.162\tau^{5.7},$$
$$y(\tau) = 1.686\tau^{0.7} + 0.531\tau^{1.7} - 1.710004\tau^{2.7} + 1.479\tau^{3.7} - 0.835\tau^{4.7} + 0.219\tau^{5.7},$$
$$z(\tau) = 0.387\tau^{0.7} - 0.788\tau^{1.7} + 0.971\tau^{2.7} - 0.8405\tau^{3.7} + 0.493\tau^{4.7} - 0.137\tau^{5.7}.$$

The estimated residual errors in the solution of symmetric Caputo fractional Rössler attractor model for various values of α are listed in Tables 7–10, representing maximum and minimum residual errors and L_2 errors. Since no comparisons and exact solutions are available for the considered model with integer order, then we have solved the considered model by using the proposed method and the fourth-order Range-Kutta method [72] for integer order. Fig. 6 provides a graphical description of the approximated solutions using the suggested approach and the fourth-order Range-Kutta method for $\alpha = 1$, demonstrating the good consistency between them. Fig. 7 represents the wavelet approximate solutions of symmetric Caputo fractional Rössler attractor model for different α. The plot of residual errors for Model 2 is depicted in Figs. 8–10 for different basis. It is evident from Fig. 6 that the outcomes closely match with the solutions obtained by using the fourth-order Range-Kutta method. When the exact solution is not available, the accuracy of the suggested scheme is demonstrated by employing the given residual error formula. The provided findings in Tables 7–10 and Figs. 8–10 also clearly show that a reduction in errors occurs when the number of USWs basis is increased.

Table 7: Estimated residual errors for Model 2 at $\alpha = 1$

τ	$x(\tau)$			$y(\tau)$			$z(\tau)$		
	$\tilde{\sigma} = 2$	$\tilde{\sigma} = 4$	$\tilde{\sigma} = 6$	$\tilde{\sigma} = 2$	$\tilde{\sigma} = 6$	$\tilde{\sigma} = 6$	$\tilde{\sigma} = 2$	$\tilde{\sigma} = 4$	$\tilde{\sigma} = 6$
0.2	1.9×10^{-3}	6.1×10^{-4}	1.1×10^{-6}	2.5×10^{-2}	5.6×10^{-4}	6.6×10^{-6}	6.9×10^{-3}	1.4×10^{-3}	1.2×10^{-5}
0.4	8.1×10^{-3}	1.4×10^{-4}	1.3×10^{-6}	4.9×10^{-2}	1.1×10^{-4}	9.1×10^{-7}	1.6×10^{-2}	2.1×10^{-4}	1.5×10^{-7}
0.6	1.2×10^{-2}	1.5×10^{-4}	2.5×10^{-6}	4.9×10^{-2}	1.1×10^{-4}	9.1×10^{-7}	2.2×10^{-2}	1.2×10^{-4}	2.9×10^{-6}
0.8	8.6×10^{-3}	9.0×10^{-4}	2.6×10^{-5}	2.5×10^{-2}	5.6×10^{-4}	6.6×10^{-6}	1.6×10^{-2}	1.1×10^{-4}	4.5×10^{-5}
1.0	7.2×10^{-2}	6.6×10^{-3}	6.2×10^{-4}	1.7×10^{-1}	3.8×10^{-3}	1.2×10^{-4}	1.4×10^{-1}	2.3×10^{-3}	1.2×10^{-3}
$RE_{\max}$	7.2×10^{-2}	6.6×10^{-3}	6.2×10^{-4}	1.7×10^{-1}	3.8×10^{-3}	1.2×10^{-4}	1.4×10^{-1}	1.1×10^{-2}	1.2×10^{-3}
$RE_{\min}$	7.4×10^{-6}	1.8×10^{-8}	1.0×10^{-7}	9.9×10^{-9}	5.6×10^{-8}	4.6×10^{-9}	4.6×10^{-7}	8.9×10^{-8}	1.1×10^{-12}
L_2	1.9×10^{-2}	1.3×10^{-3}	8.6×10^{-5}	7.2×10^{-2}	1.0×10^{-3}	2.4×10^{-5}	3.9×10^{-2}	2.1×10^{-3}	1.7×10^{-4}

Table 8: Estimated residual errors for Model 2 at $\alpha = 0.9$

τ	$x(\tau)$			$y(\tau)$			$z(\tau)$		
	$\tilde{\sigma} = 2$	$\tilde{\sigma} = 4$	$\tilde{\sigma} = 6$	$\tilde{\sigma} = 2$	$\tilde{\sigma} = 4$	$\tilde{\sigma} = 6$	$\tilde{\sigma} = 2$	$\tilde{\sigma} = 4$	$\tilde{\sigma} = 6$
0.2	1.4×10^{-2}	7.9×10^{-4}	1.4×10^{-4}	2.8×10^{-2}	8.9×10^{-5}	7.6×10^{-5}	1.1×10^{-2}	1.2×10^{-3}	2.5×10^{-4}
0.4	2.8×10^{-2}	2.0×10^{-4}	1.4×10^{-5}	5.2×10^{-2}	1.5×10^{-5}	6.8×10^{-6}	2.5×10^{-2}	6.4×10^{-5}	3.2×10^{-5}
0.6	3.1×10^{-2}	2.2×10^{-4}	1.3×10^{-5}	5.1×10^{-2}	3.2×10^{-5}	5.2×10^{-6}	3.2×10^{-2}	6.1×10^{-5}	3.3×10^{-5}
0.8	1.7×10^{-2}	1.1×10^{-3}	9.3×10^{-5}	2.6×10^{-2}	2.1×10^{-4}	3.1×10^{-5}	2.0×10^{-2}	7.8×10^{-4}	2.5×10^{-4}
1.0	1.2×10^{-1}	8.0×10^{-3}	1.6×10^{-3}	1.7×10^{-1}	1.6×10^{-3}	4.8×10^{-4}	1.6×10^{-1}	7.5×10^{-3}	4.7×10^{-3}
$RE_{\max}$	1.2×10^{-1}	8.0×10^{-3}	1.1×10^{-2}	2.1×10^{-1}	7.4×10^{-3}	5.7×10^{-3}	1.6×10^{-1}	2.2×10^{-2}	1.1×10^{-2}
$RE_{\min}$	5.7×10^{-8}	1.4×10^{-7}	3.4×10^{-7}	2.2×10^{-1}	1.9×10^{-8}	9.6×10^{-8}	7.4×10^{-6}	1.2×10^{-7}	7.9×10^{-8}
L_2	4.6×10^{-2}	1.6×10^{-3}	1.1×10^{-3}	7.8×10^{-2}	9.0×10^{-4}	5.7×10^{-4}	5.0×10^{-2}	3.4×10^{-3}	1.3×10^{-3}

Table 9: Estimated residual errors for Model 2 at $\alpha = 0.8$

τ	$x(\tau)$			$y(\tau)$			$z(\tau)$		
	$\tilde{\sigma} = 2$	$\tilde{\sigma} = 4$	$\tilde{\sigma} = 6$	$\tilde{\sigma} = 2$	$\tilde{\sigma} = 4$	$\tilde{\sigma} = 6$	$\tilde{\sigma} = 2$	$\tilde{\sigma} = 4$	$\tilde{\sigma} = 6$
0.2	2.6×10^{-2}	1.1×10^{-4}	2.9×10^{-4}	2.8×10^{-2}	1.3×10^{-3}	1.8×10^{-4}	1.5×10^{-2}	9.2×10^{-4}	5.1×10^{-4}
0.4	4.8×10^{-2}	1.0×10^{-4}	2.5×10^{-5}	5.1×10^{-2}	1.7×10^{-4}	1.6×10^{-5}	3.3×10^{-2}	5.2×10^{-6}	5.5×10^{-5}
0.6	4.7×10^{-2}	1.3×10^{-4}	1.9×10^{-5}	4.9×10^{-2}	1.2×10^{-4}	1.2×10^{-5}	3.9×10^{-2}	8.2×10^{-5}	4.8×10^{-5}
0.8	2.4×10^{-2}	6.6×10^{-4}	1.1×10^{-4}	2.5×10^{-2}	5.1×10^{-4}	7.0×10^{-5}	2.3×10^{-2}	5.4×10^{-4}	3.2×10^{-4}
1.0	1.6×10^{-1}	4.2×10^{-3}	1.8×10^{-3}	1.6×10^{-1}	2.8×10^{-3}	1.0×10^{-3}	1.7×10^{-1}	3.5×10^{-3}	5.4×10^{-3}
$RE_{\max}$	2.5×10^{-1}	3.6×10^{-2}	3.2×10^{-2}	2.2×10^{-1}	2.8×10^{-2}	1.5×10^{-2}	1.7×10^{-1}	3.7×10^{-2}	2.8×10^{-2}
$RE_{\min}$	8.6×10^{-8}	1.2×10^{-7}	1.0×10^{-7}	4.1×10^{-8}	1.6×10^{-7}	1.4×10^{-7}	2.2×10^{-8}	1.1×10^{-16}	5.8×10^{-8}
L_2	7.7×10^{-2}	3.5×10^{-3}	2.9×10^{-3}	7.8×10^{-2}	3.6×10^{-3}	1.5×10^{-3}	5.8×10^{-2}	4.6×10^{-3}	2.9×10^{-3}

Table 10: Estimated residual errors for Model 2 at $\alpha = 0.7$

τ	$x(\tau)$			$y(\tau)$			$z(\tau)$		
	$\tilde{\sigma} = 2$	$\tilde{\sigma} = 4$	$\tilde{\sigma} = 6$	$\tilde{\sigma} = 2$	$\tilde{\sigma} = 4$	$\tilde{\sigma} = 6$	$\tilde{\sigma} = 2$	$\tilde{\sigma} = 4$	$\tilde{\sigma} = 6$
0.2	3.7×10^{-2}	2.0×10^{-3}	4.7×10^{-4}	2.5×10^{-2}	3.1×10^{-3}	3.7×10^{-4}	1.8×10^{-2}	1.6×10^{-3}	5.7×10^{-4}
0.4	6.3×10^{-2}	2.2×10^{-4}	3.5×10^{-5}	4.5×10^{-2}	4.4×10^{-4}	3.3×10^{-5}	3.8×10^{-2}	2.1×10^{-4}	5.0×10^{-5}
0.6	5.9×10^{-2}	1.7×10^{-4}	2.4×10^{-5}	4.2×10^{-2}	3.6×10^{-4}	2.4×10^{-5}	4.1×10^{-2}	2.2×10^{-4}	3.8×10^{-5}
0.8	2.9×10^{-2}	7.4×0^{-4}	1.3×10^{-4}	2.1×10^{-2}	1.5×10^{-3}	1.4×10^{-4}	2.3×10^{-2}	1.3×10^{-3}	2.3×10^{-4}
1.0	1.9×10^{-1}	4.6×10^{-3}	1.9×10^{-3}	1.4×10^{-1}	9.4×10^{-3}	2.2×10^{-3}	1.6×10^{-1}	1.0×10^{-2}	3.7×10^{-3}
$RE_{\max}$	4.0×10^{-1}	9.3×10^{-2}	6.8×10^{-2}	2.1×10^{-1}	5.8×10^{-2}	3.2×10^{-2}	1.6×10^{-1}	6.0×10^{-2}	4.8×10^{-2}
$RE_{\min}$	1.3×10^{-9}	2.2×10^{-7}	2.9×10^{-13}	1.8×10^{-6}	2.0×10^{-8}	2.4×10^{-13}	1.2×10^{-8}	2.0×10^{-7}	9.5×10^{-8}
L_2	1.0×10^{-1}	9.5×10^{-3}	5.6×10^{-3}	6.9×10^{-2}	7.6×10^{-3}	3.0×10^{-3}	6.2×10^{-2}	7.0×10^{-3}	4.4×10^{-3}

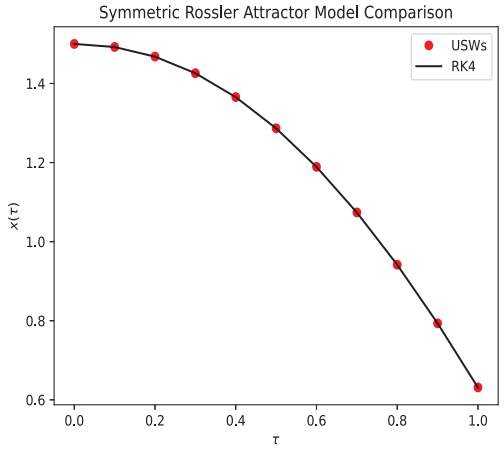

(a) $x(\tau)$

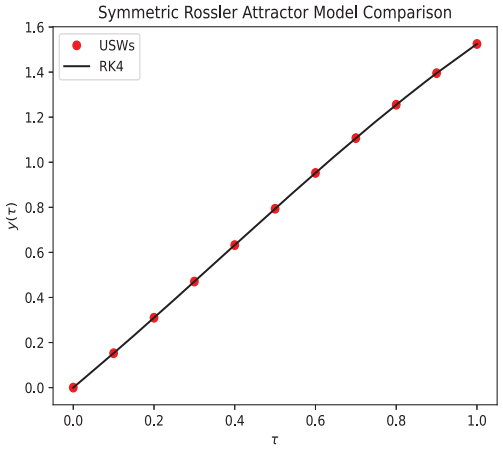

(b) $y(\tau)$

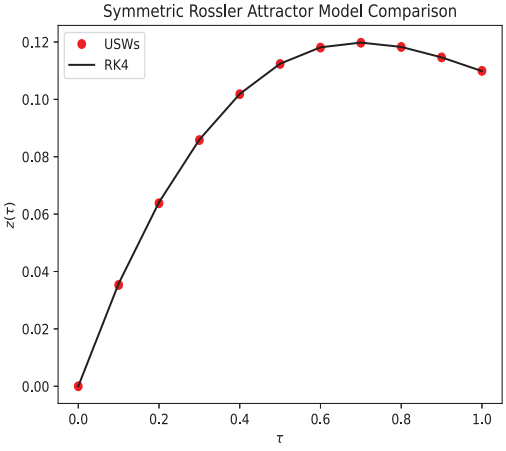

(c) $z(\tau)$

Figure 6: Solution of Model 2 via the suggested approach with fourth-order Range-Kutta method at $\alpha = 1$ & $\tilde{\sigma} = 4$

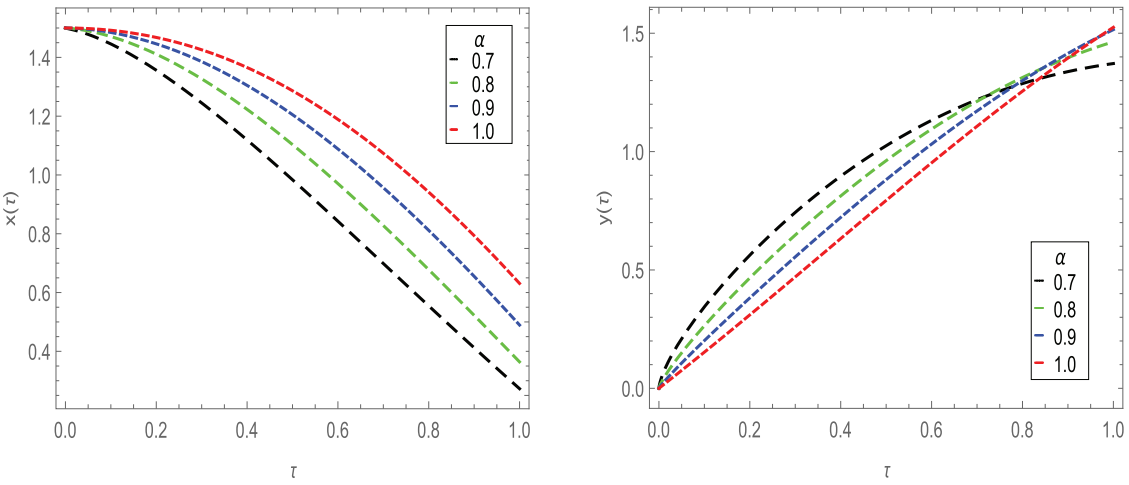

(a) $x(\tau)$ (b) $y(\tau)$

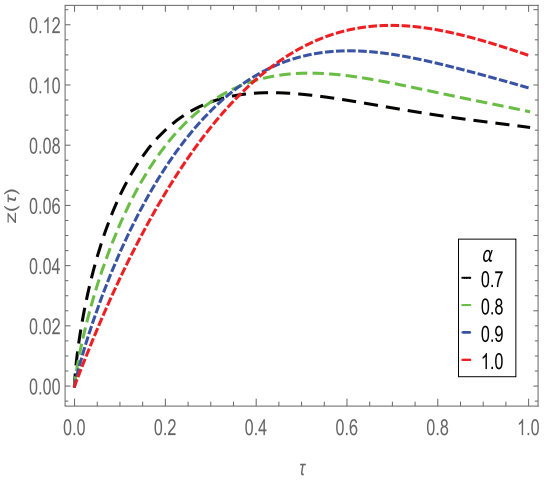

(c) $z(\tau)$

Figure 7: Solution of Model 2 for different α and $\tilde{\sigma} = 6$

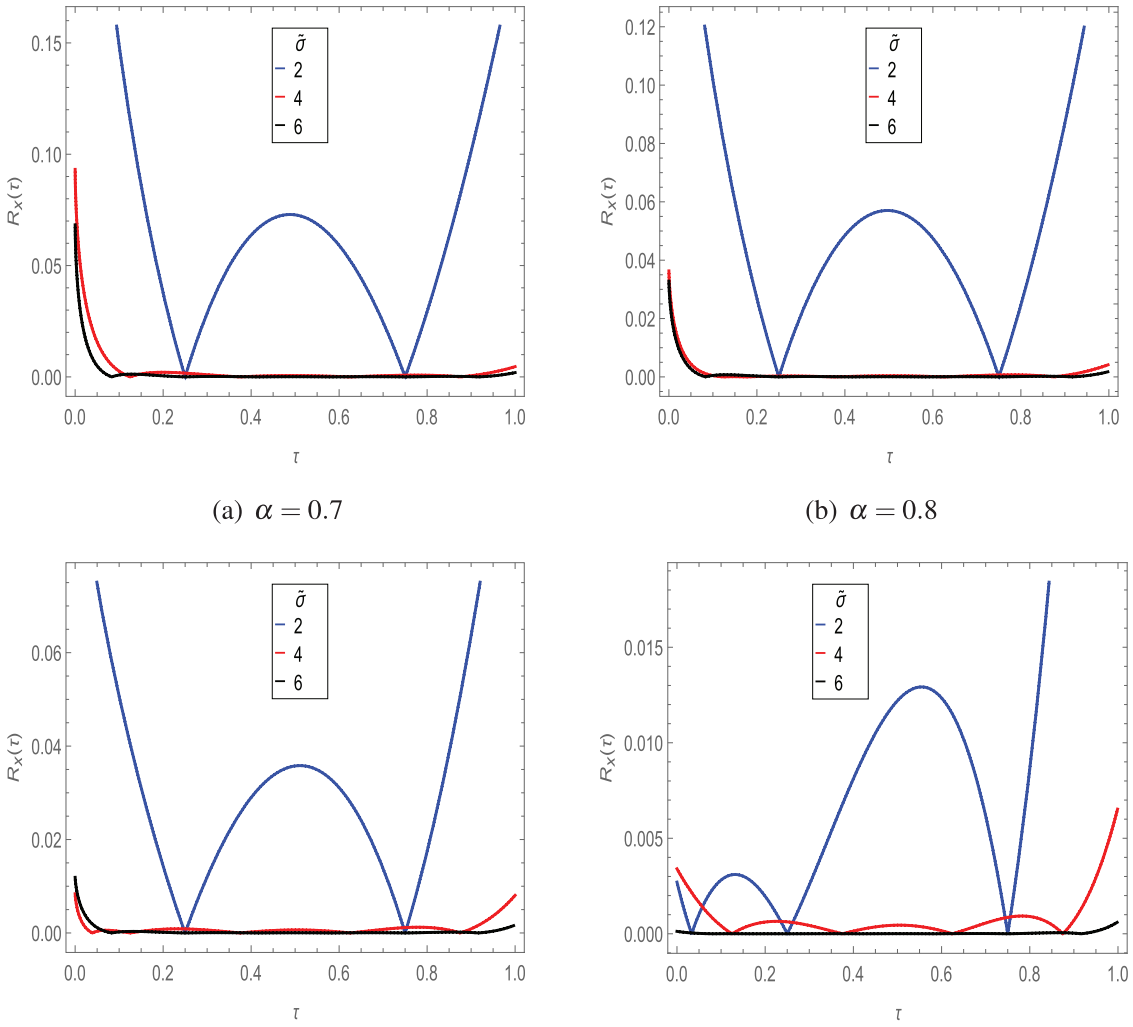

(a) $\alpha = 0.7$ (b) $\alpha = 0.8$

(c) $\alpha = 0.9$ (d) $\alpha = 1.0$

Figure 8: Residual error in $x(\tau)$ of Model 2 for different α and $\tilde{\sigma}$

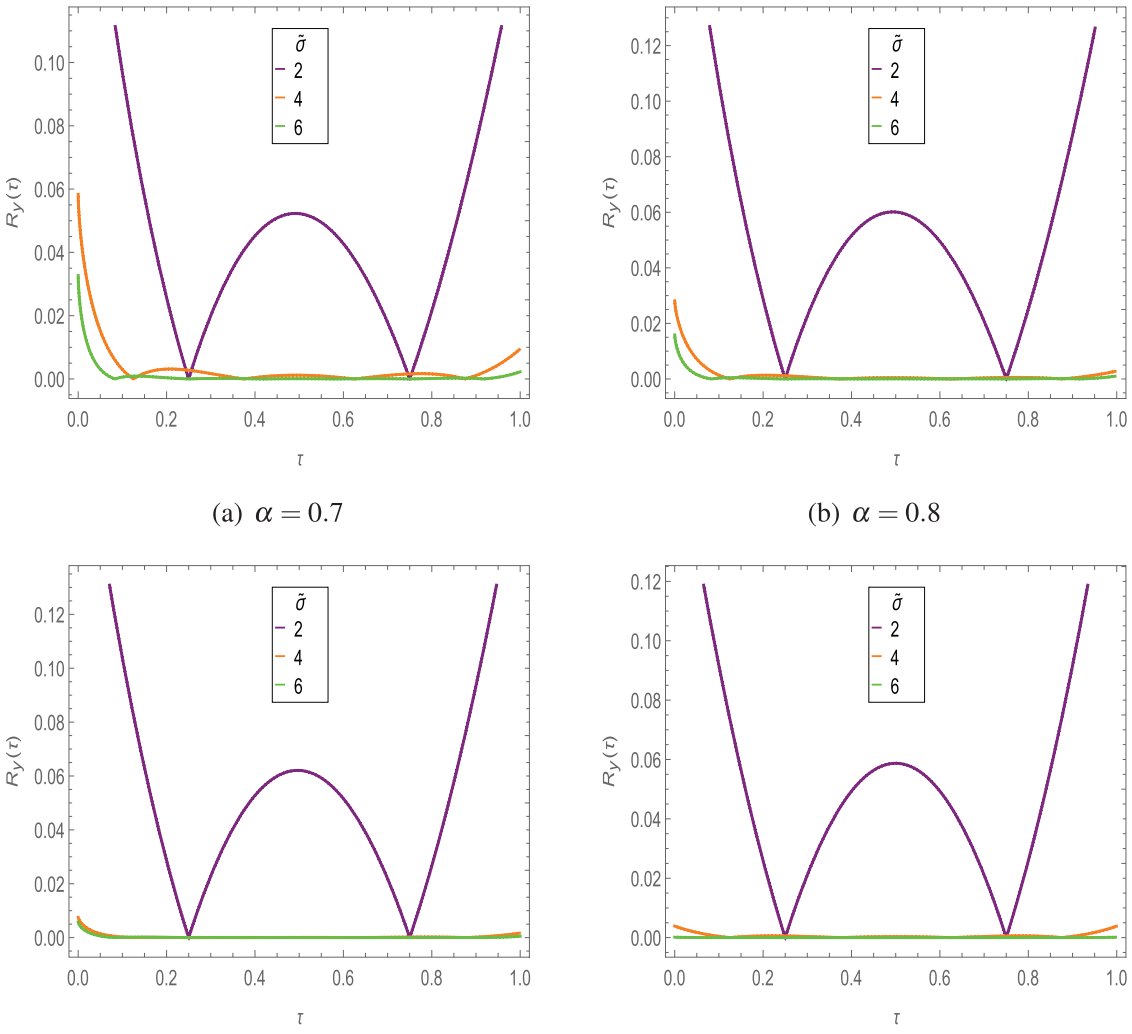

(a) $\alpha = 0.7$ (b) $\alpha = 0.8$

(c) $\alpha = 0.9$ (d) $\alpha = 1.0$

Figure 9: Residual error in $y(\tau)$ of Model 2 for different α and $\tilde{\sigma}$

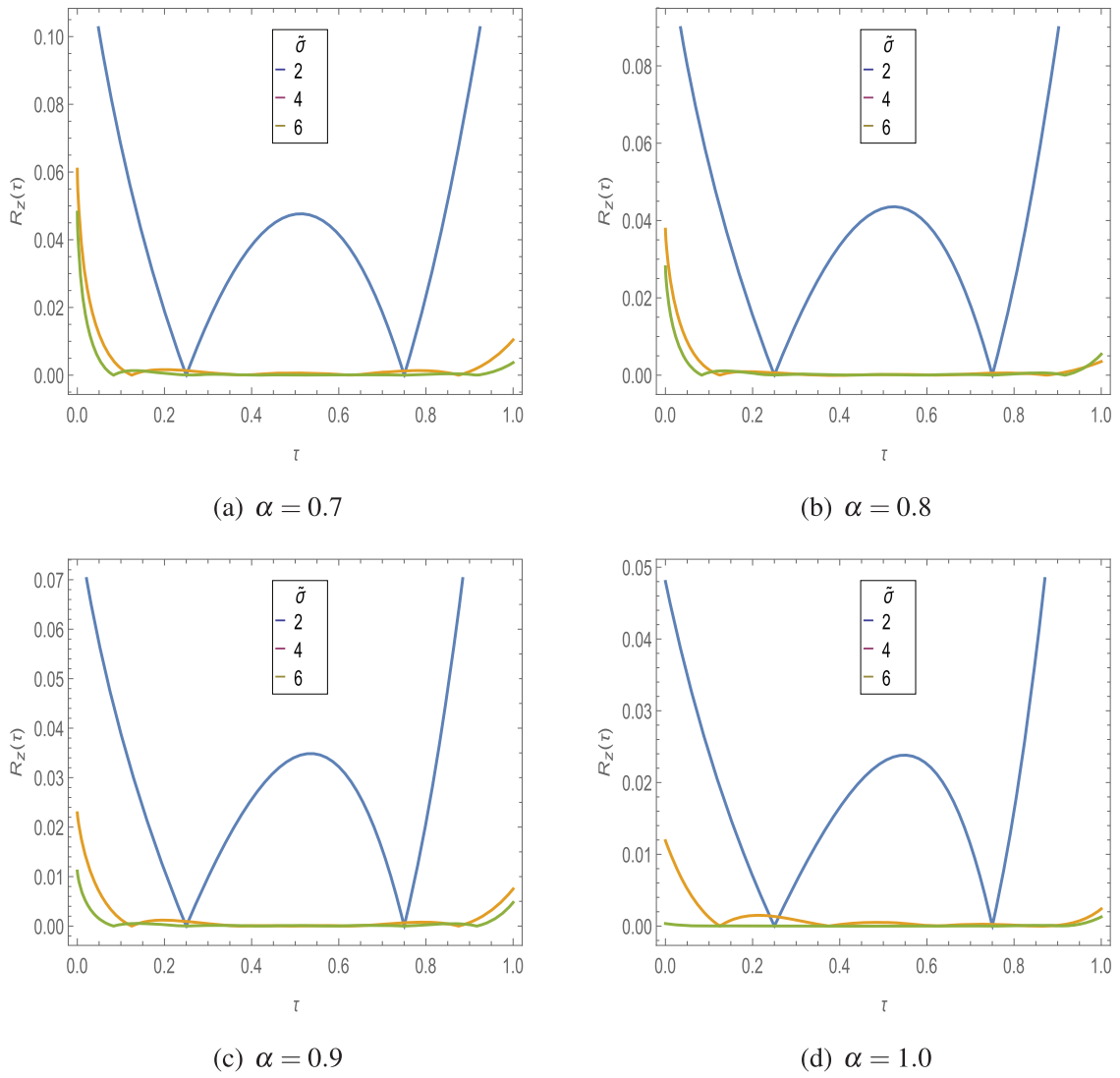

Figure 10: Residual error in $z(\tau)$ of Model 2 for different α and $\tilde{\sigma}$

7 Conclusions

In this work, we investigated the dynamical behavior of the Caputo fractional Rössler attractor model using the Caputo differential operator, which inherits almost all features of the integer-order Rössler chaotic system in its dynamic properties. The Caputo fractional Rössler attractor model has been numerically investigated using the USWs approach which effectively and conveniently displays the solutions and residual errors. The success of the USWs-based approach in computing the accurate error for the Caputo fractional Rössler attractor model suggests that this approach has the potential to be employed in several other areas of engineering and technology. The exactness dependability of the Caputo fractional Rössler attractor model has been verified through L_2 error & residual error. From the above Figures and Tables, it can be easily seen that the USWs basis functions well as shown by the obtained low error values. The approach presented here shortens calculation complexity, streamlines the process, and yields better results. The results obtained by the proposed method for fractional order will be useful for further investigations in the applications of nonlinear Caputo fractional Rössler attractor model as well as for comparison purposes. The outcomes

of this study contribute to the advancement of the dynamical system and can be used in the future to find the efficient solution of systems of higher-dimension multi-delay differential equations under multiple boundary conditions.

The study's reliance on USWs offers computational advantages but may lead to high costs for large systems. Additionally, the scheme's focus on a limited domain restricts broader applicability, and dynamic behaviors like bifurcations and stability remain underexplored, limiting the study's generalizability.

Acknowledgement: None.

Funding Statement: "La derivada fraccional generalizada, nuevos resultados y aplicaciones a desigualdades integrales" Cod UIO-077-2024. This study is supported via funding from Prince Sattam bin Abdulaziz University project number (PSAU/2025/R/1446).

Author Contributions: Conceptualization, Ashish Rayal and Priya Dogra; Formal analysis, Ashish Rayal, Priya Dogra, Sabri T. M. Thabet, Imed Kedim and Miguel Vivas-Cortez; Funding acquisition, Miguel Vivas-Cortez; Investigation, Ashish Rayal, Priya Dogra, Sabri T. M. Thabet, Imed Kedim and Miguel Vivas-Cortez; Methodology, Ashish Rayal, Priya Dogra, Sabri T. M. Thabet, Imed Kedim and Miguel Vivas-Cortez; Software, Ashish Rayal and Priya Dogra; Validation, Ashish Rayal, Priya Dogra, Sabri T. M. Thabet and Imed Kedim; Writing—original draft, Ashish Rayal, Priya Dogra, Sabri T. M. Thabet, Imed Kedim and Miguel Vivas-Cortez; Writing—review & editing, Ashish Rayal, Priya Dogra, Sabri T. M. Thabet, Imed Kedim and Miguel Vivas-Cortez. All authors reviewed the results and approved the final version of the manuscript.

Availability of Data and Materials: All data generated or analyzed during this study are included in this published article.

Ethics Approval: Not applicable.

Conflicts of Interest: The authors declare no conflicts of interest to report regarding the present study.

References

1. Fleuren LM, Klausch TLT, Zwager CL, Schoonmade LJ, Guo T, Roggeveen LF, et al. Machine learning for the prediction of sepsis: a systematic review and meta-analysis of diagnostic test accuracy. Intensive Care Med. 2020;46(3):383–400. doi:10.1007/s00134-019-05872-y.
2. Arefin S, Chowdhury M, Parvez R, Ahmed T, Abrar AFMS, Sumaiya F. Understanding APT detection using Machine learning algorithms: is superior accuracy a thing?. In: 2024 IEEE International Conference on Electro Information Technology (eIT); 2024; Eau Claire, WI, USA. p. 532–7.
3. Mora HM, Pont MT, Lopez FA, Pascual JM, Chamizo JM. Advancements in number representation for high-precision computing. J Super Comput. 2024;80(7):9742–61. doi:10.1007/s11227-023-05814-y.
4. Madaliev M, Orzimatov J, Abdulkhaev Z, Esonov O, Mirzaraximov M. Several different ways to increase the accuracy of the numerical solution of the first order wave equation. BIO Web of Conf. 2024;84(2):02032. doi:10.1051/bioconf/20248402032.
5. Debnath L. A brief historical introduction to fractional calculus. Int J Mathem Educat Sci Technol. 2004;35(4):487–501. doi:10.1080/00207390410001686571.
6. Mani G, Gnanaprakasam AJ, Guran L, George R, Mitrovi'c ZD. Some results in fuzzy b-metric space with b-triangular property and applications to Fredholm integral equations and dynamic programming. Mathematics. 2023;11(19):4101. doi:10.3390/math11194101.
7. Mani G, Gnanaprakasam AJ, Ege O, Aloqaily A, Mlaiki N. Fixed point results inC^*-algebra-valued partial b-metric spaces with related application. Mathematics. 2023;11(5):1158. doi:10.3390/math11051158.
8. Mani G, Haque S, Gnanaprakasam AJ, Ege O, Mlaiki N. The study of bicomplex-valued controlled metric spaces with applications to fractional differential equations. Mathematics. 2023;11(12):2742. doi:10.3390/math11122742.

9. Ross B. A brief history and exposition of the fundamental theory of fractional calculus. In: Ross B, editor. Fractional calculus and its applications. Lecture notes in mathematics. Berlin/Heidelberg: Springer; 1975.
10. Singh AP, Deb D, Agrawal H, Bingi K, Ozana S. Modeling and control of robotic manipulators: a fractional calculus point of view. Arab J Sci Eng. 2021;46(10):9541–52. doi:10.1007/s13369-020-05138-6.
11. Wang H. Research on application of fractional calculus in signal real-time analysis and processing in stock financial market. Chaos, Solit Fract. 2019;128(1):92–7. doi:10.1016/j.chaos.2019.07.021.
12. Wang Q, Ma J, Yu S, Tan L. Noise detection and image denoising based on fractional calculus. Chaos Solit Fract. 2020;131(4):109463. doi:10.1016/j.chaos.2019.109463.
13. Baleanu D, Sajjadi SS, Jajarmi A, Defterli O. On a nonlinear dynamical system with both chaotic and nonchaotic behaviors: a new fractional analysis and control. Adv Differ Equ. 2021;234(1):148. doi:10.1186/s13662-021-03393-x.
14. Ben-loghfyry A, Hakim A. Reaction-diffusion equation based on fractional-time anisotropic diffusion for textured images recovery. Int J Appl Comput Math. 2022;8(4):177. doi:10.1007/s40819-022-01380-8.
15. Yang X, Gao F, Ju Y. General fractional derivatives with applications in viscoelasticity. Netherlands: Elsevier Science; 2020.
16. Tang TQ, Shah Z, Jan R, Alzahrani E. Modeling the dynamics of tumor-immune cells interactions via fractional calculus. Eur Phys J Plus. 2022;137(3):367. doi:10.1140/epjp/s13360-022-02591-0.
17. Viera-Martin E, Gomez-Aguilar JF, Solis-Perez JE, Hernandez-Perez JA, Escobar-Jimenez RF. Artificial neural networks: a practical review of applications involving fractional calculus. Eur Phys J Spec Top. 2022;231(10):2059–95. doi:10.1140/epjs/s11734-022-00455-3.
18. Harrouche N, Momani S, Hasan S, Al-Smadi M. Computational algorithm for solving drug pharmacokinetic model under uncertainty with nonsingular kernel type Caputo-Fabrizio fractional derivative. Alexandria Eng J. 2021;60(5):4347–62. doi:10.1016/j.aej.2021.03.016.
19. Cristofaro L, Garra R, Scalas E, Spassiani I. A fractional approach to study the pure-temporal Epidemic Type Aftershock Sequence (ETAS) process for earthquakes modeling. Fract Calc Appl Anal. 2023;26(2):461–79. doi:10.1007/s13540-023-00144-5.
20. Gorenflo R, Mainardi F. Fractional calculus: integral and differential equations of fractional order. Austria: Springer Vienna; 1997.
21. Odibat ZM, Al-Refai MA, Baleanu D. On some properties of generalized cardinal sine kernel fractional operators: advantages and applications of the extended operators. Chin J Phys. 2024;91: 349–60.
22. Shams M, Kausar N, Agarwal P, Jain S. Fuzzy fractional Caputo-type numerical scheme for solving fuzzy nonlinear equations. Fract Differ Equat, Acad Press. 2024;2(5):167–75. doi:10.1016/B978-0-44-315423-2.00016-3.
23. Owolabi KM. Efficient numerical simulation of non-integer-order space-fractional reaction-diffusion equation via the Riemann-Liouville operator. The Eur Phys J Plus. 2018;133(3):1–16. doi:10.1140/epjp/i2018-11951-x.
24. Jiang Y, Zhang B. Comparative study of Riemann-Liouville and Caputo derivative definitions in time-domain analysis of fractional-order capacitor. IEEE Transact Circ Syst II: Express Briefs. 2020;67(10):2184–8. doi:10.1109/TCSII.2019.2952693.
25. Ghosh B, Mohapatra J. Analysis of finite difference schemes for Volterra integro-differential equations involving arbitrary order derivatives. J Appl Math Comput. 2023;69(2):1865–86. doi:10.1007/s12190-022-01817-9.
26. Thabet STM, Dhakne MB. Nonlinear fractional integro-differential equations with two boundary conditions. Adv Studies Contemp Mathem. 2016;26(3):513–26.
27. Thabet STM, Dhakne MB. On boundary value problems of higher order abstract fractional integro-differential equations. Int J Nonl Anal Applicat. 2016;7(2):165–84. doi:10.22075/ijnaa.2017.520.
28. Liu L, Chen S, Feng L, Zhu J, Zhang J, Zheng L, et al. A novel distributed order time fractional model for heat conduction, anomalous diffusion, and viscoelastic flow problems. Comput Fluids. 2023;265:105991. doi:10.1016/j.compfluid.2023.105991.
29. Abdou MA. An analytical method for space-time fractional nonlinear differential equations arising in plasma physics. J Ocean Eng Sci. 2017;2(4):288–92. doi:10.1016/j.joes.2017.09.002.
30. Alam M, Zada A, Abdeljawad T. Stability analysis of an implicit fractional integro-differential equation via integral boundary conditions. Alexandria Eng J. 2024;87(4):501–14. doi:10.1016/j.aej.2023.12.055.

31. Thabet STM, Kedim I. Study of nonlocal multiorder implicit differential equation involving Hilfer fractional deriva-tive on unbounded domains. J Math. 2023;2023(3):1–14. doi:10.1155/2023/8668325.
32. Rehman ZU, Boulaaras SM, Jan R, Ahmad I, Bahramand S. Computational analysis of financial system through non-integer derivative. J Comput Sci. 2023;75(12):102204. doi:10.1016/j.jocs.2023.102204.
33. Dhobale SM, Chatterjee S. A general class of optimal nonlinear resonant controllers of fractional order with time-delay for active vibration control-theory and experiment. Mech Syst Signal Process. 2023;182(11):109580. doi:10.1016/j.ymssp.2022.109580.
34. Rayal A, Negi P, Giri S, Baskonus HM. Taylor wavelet analysis and numerical simulation for boundary value problems of higher order under multiple boundary conditions. Pramana-J Phys. 2024;98(4):155. doi:10.1007/s12043-024-02825-z.
35. Rayal A, Anand M, Srivastava VK. Application of fractional modified Taylor wavelets in the dynamical analysis of fractional electrical circuits under generalized Caputo fractional derivative. Phys Scr. 2024;99(12):125255. doi:10.1088/1402-4896/ad8701.
36. Young RK. Wavelet theory and its applications. 1st ed. New York, NY, USA: Springer Science & Business Media; 2012.
37. Youssri YH, Abd-Elhameed WM, Doha EH. Ultraspherical wavelets method for solving Lane-Emden type equations. Rom J Phys. 2015;60(9–10):1298–314.
38. Farge M. Wavelet transforms and their applications to turbulence. Annual Rev Fluid Mech. 1992;24(1):395–458. doi:10.1146/annurev.fl.24.010192.002143.
39. Rayal A, Verma SR. Numerical study of variational problems of moving or fixed boundary conditions by Muntz wavelets. J Vibrat Control. 2020;28:1–16. doi:10.1177/10775463209747.
40. Rayal A, Patel PA, Giri S, Joshi P. A Comparative study of a class of Linear and Nonlinear Pantograph Differential Equations via different orthogonal polynomial Wavelets. Malaysian J Sci. 2024;43(2):75–95. doi:10.22452/mjs.vol43no2.9.
41. Rayal A, Joshi P. A comprehensive review on fractional operators, wavelets, and their applications. Redshine Archive. 2024;11(4):380–7.
42. Rayal A, Bisht P, Giri S, Patel PA, Prajapati M. Dynamical analysis and numerical treatment of pond pollution model endowed with Caputo fractional derivative using effective wavelets technique. Int J Dyn Control. 2024;2024(12):1–14. doi:10.1007/s40435-024-01494-5.
43. Rayal A, Verma SR. Two-dimensional Gegenbauer wavelets for the numerical solution of tempered fractional model of the nonlinear Klein-Gordon equation. Appl Numer Math. 2022;174(10):191–220. doi:10.1016/j.apnum.2022.01.015.
44. Rayal A, Anand M, Chauhan K, Prinsa. An overview of mamadu-njoseh wavelets and its properties for numerical computations. Uttaranchal J Appl Life Sci. 2023;4(1):1–8.
45. Rayal A. An effective Taylor wavelets basis for the evaluation of numerical differentiations. Palestine J Mathem. 2023;12:551–68.
46. Rayal A. Muntz wavelets solution for the polytropic lane-emden differential equation involved with conformable type fractional derivative. Int J Appl Comput Math. 2023;9(4):50. doi:10.1007/s40819-023-01528-0.
47. Rayal A, Joshi BP, Pandey M, Torres DFM. Numerical investigation of the fractional oscillation equations under the context of variable order caputo fractional derivative via fractional order bernstein wavelets. Mathematics. 2023;11(11):2503. doi:10.3390/math11112503.
48. Rayal A, Verma SR. Numerical analysis of pantograph differential equation of the stretched type associated with fractal-fractional derivatives via fractional order Legendre wavelets. Chaos Solit Fract. 2020;139(1):110076. doi:10.1016/j.chaos.2020.110076.
49. Devaney RL. An introduction to chaotic dynamical systems. Boca Raton, FL, USA: CRC Press; 2021.
50. Atangana A, Qureshi S. Modeling attractors of chaotic dynamical systems with fractal-fractional operators. Chaos Solit Fract. 2019;123(3):320–37. doi:10.1016/j.chaos.2019.04.020.

51. Shen BW, Pielke SRRA, Zeng X, Baik JJ, Faghih-Naini S, Cui J, et al. Is weather chaotic? Coexisting chaotic and non-chaotic attractors within Lorenz models. Vol. 13. In: 13th Chaotic Modeling and Simulation International Conference. Springer Proceedings in Complexity. Cham: Springer; 2021. p. 805–25.
52. Desharnais RA, Henson SM, Costantino RF, Dennis B. Capturing chaos: a multidisciplinary approach to nonlinear population dynamics. J Differ Equat Applicat. 2023;30(8):1002–39. doi:10.1080/10236198.2023.2260013.
53. Lahmiri S. Assessing efficiency in prices and trading volumes of cryptocurrencies before and during the COVID-19 pandemic with fractal, chaos, and randomness: evidence from a large dataset. Financ Innovation. 2024;10(1):82. doi:10.1186/s40854-024-00628-0.
54. Zhang B, Liu L. Chaos-based image encryption: review, application, and challenges. Mathematics. 2023;11(11):2585. doi:10.3390/math11112585.
55. Shen BW. A review of lorenz's models from 1960 to 2008. Int J Bifurcat Chaos. 2023;33(10):2330024. doi:10.1142/S0218127423300240.
56. Corona-Bermudez E, Chimal-Eguia JC, Corona-Bermudez U, Rivero-Angeles ME. Chaos meets cryptography: developing an S-box design with the rössler attractor. Mathematics. 2023;11(22):4575. doi:10.3390/math11224575.
57. Rössler OE. An equation for continuous chaos. Phys Letters A. 1976;57:397–8.
58. Li C, Hu W, Sprott JC, Wang X. Multistability in symmetric chaotic systems. Eur Phys J Spec Top. 2015;224(8):1493–506. doi:10.1140/epjst/e2015-02475-x.
59. Kontorovich VY, Beltran LA, Aguilar JM, Lovtchikova Z, Tinsley KR. Cumulant analysis of Rössler attractor and its applications. The Open Cybernet Syst J. 2009;3:29–39.
60. Rysak A, Sedlmayr M, Gregorczyk M. Revealing fractionality in the Rössler system by recurrence quantification analysis. The Eur Phy J Spec Topics. 2023;232(1):83–98. doi:10.1140/epjs/s11734-022-00740-1.
61. Elbadri M, Abdoon MA, Berir M, Almutairi DK. A numerical solution and comparative study of the symmetric rossler attractor with the generalized caputo fractional derivative via two different methods. Mathematics. 2023;11(13):2997. doi:10.3390/math11132997.
62. Kekana MC, Shatalov MY, Tong TO, Fadugba SE. Analysis of Rossler attractor by means of residual and Joubert-Greeff methods. South East Asian J Mathem Mathem Sci. 2023;19(02):431–50. doi:10.56827/SEAJMMS.2023.1902.32.
63. Barrio R, Blesa F, Serrano S. Qualitative analysis of the Rössler equations: bifurcations of limit cycles and chaotic attractors. Physica D: Nonlin Phenom. 2009;238(13):1087–100. doi:10.1016/j.physd.2009.03.010.
64. Santra MS, Gaur SS, Gupta A. Numerical solution of Rössler attractor using power series method. Int Res J Adv Eng Manag. 2024;2(3):182–6. doi:10.47392/IRJAEM.2024.0028.
65. Boulehmi K. A novel numerical scheme for fractional bernoulli equations and the Rössler model: a comparative analysis using atangana-baleanu caputo fractional derivative. Eur J Pure Appl Mathem. 2024;17(1):445–61. doi:10.29020/nybg.ejpam.v17i1.5043.
66. Odibat ZM, Baleanu D. Numerical simulation of initial value problems with generalized Caputo-type fractional derivatives. Appl Num Mathem. 2020;156(6):94–105. doi:10.1016/j.apnum.2020.04.015.
67. Askey R, Ismail MEH. A generalization of ultraspherical polynomials. Birkhäuser Basel, Switzerland, 1983.
68. Abd-Elhameed WM, Youssri YH. New spectral solutions of multi-term fractional-order initial value problems with error analysis. Comput Model Eng Sci. 2015;105(5):375–98. doi:10.3970/cmes.2015.105.375.
69. Ozdemir N, Secer A. A numerical algorithm based on ultraspherical wavelets for solution of linear and nonlinear Klein Gordon equations. Sigma J Eng Natural Sci. 2020;38(3):1307–19.
70. Artin E. The gamma function. Garden City, NY, USA: Dover Publications; 2015.
71. Tavazoei MS, Haeri M. Chaotic attractors in incommensurate fractional order systems. Physica D. 2008;237(20):2628–37. doi:10.1016/j.physd.2008.03.037.
72. Mehdi SA, Kareem RS. Using fourth-order Runge-kutta method to solve lu chaotic system. Am J Eng Res. 2017;6(1):72–7.